2012

Gibbs Energy Modeling of Binary and Ternary Molten Nitrate Salt Systems

Tucker Elliott
Lehigh University

Gibbs Energy Modeling of Binary and Ternary Molten Nitrate Salt Systems

by

Tucker R. Elliott

A Thesis

Presented to the Graduate and Research Committee

of Lehigh University

in Candidacy for the Degree of

Master of Science

in

Mechanical Engineering and Mechanics

Lehigh University

November 2011

This thesis is accepted and approved in partial fulfillment of the requirements for the Master of Science.

Gibbs Energy Modeling of Binary and Ternary Molten Nitrate Salt Systems

_____

Date Approved

_____

Dr. Alparslan Oztekin
Advisor

_____

Dr. Sudhakar Neti
Co-Advisor

_____

Dr. D. Gary Harlow
Department Chairperson

ACKNOWLEDGEMENTS

I would like to thank Dr. Alparslan Oztekin and Dr. Sudhakar Neti for their continuous support throughout this research project and their guidance regarding this thesis. They have been an invaluable source of information. Additionally, I would like to thank Dr. Satish Mohapatra and Dynalene Inc. for sponsoring the project, as well providing suggestions and experimental data to improve my work.

Finally, I would like to thank Walter and Patti Ann, my father and mother, who enabled me to be in the position that I am today.

TABLE OF CONTENTS

Page

List of Figures

Page

List of Tables

Page

Abstract

Molten nitrate salts have the potential to become efficient heat transfer fluids in many applications, including concentrated solar power plants and in energy storage systems. Their low melting temperatures and high energy densities contribute to this. Thus, an understanding of the phase diagrams of these salts is important, specifically, knowledge of the melting and freezing temperatures of these mixtures at various concentrations. Many previous works have investigated modeling these phase diagrams, particularly binary mixtures of nitrate salts. Ternary simulations for molten salts exist but results have been limited. Using existing enthalpy of mixing data for binary mixtures, an accurate ternary phase diagram has been constructed. The binary systems $NaNO_3$- KNO_3, $LiNO_3$- $NaNO_3$, and $LiNO_3$- KNO_3 and the ternary system $LiNO_3$-$NaNO_3$-KNO_3 have been modeled using a Gibbs energy minimization method. The predictions from this present model agree well with the results of experiments by our group and the data collected by previous researchers. The ternary predictions constructed using only binary interactions, agree reasonably well with the experimental data collected by our group. It is determined that the ternary mixture has a eutectic temperature of 107° Celsius at a composition of 43-47-10 mole percent $LiNO_3$-KNO_3-$NaNO_3$ respectively, and will be a viable heat transfer fluid. The thermodynamic model used here can be applied to any ternary system as well as any higher-order component system.

Chapter 1. Introduction

As the world looks to decrease fossil fuel usage, the need for a clean renewable energy source has become more apparent. Solar thermal energy is one such alternative energy choice. In 2007, of all the energy utilized in the United States, only 7% came from renewable sources. And of that, only 1% was from solar sources [1]. The market for solar thermal energy is therefore young. For solar thermal energy to become a more viable technology, a heat transfer fluid with a high energy density and low melting point is desired. The molten nitrate salts presented here have such qualities. Binary and ternary systems of nitrate salts have lower melting temperatures than single component nitrate salts and as a result need less inputted energy to remain molten. During the night or a cloudy day, when no sunlight is available, less energy from the grid is needed to heat the fluid. This can keep costs down for a solar power plant, for example. In addition, using the eutectic composition of a binary or ternary salt, means the lowest melting point of that salt is utilized. Therefore at the eutectic temperature, the smallest amount of inputted energy is needed to keep the salt in the liquid state. Nitrate salts were chosen over other salts for their high energy density, stability at high temperatures, and their relatively low melting points [2].

Molten salts can be used in different solar thermal applications as heat transfer fluids. One example is in a parabolic trough system. The molten salt flows through a piping scheme which is placed at the focal point of a parabolic mirror. The sun's rays are deflected from the mirror and are focused on the tube so that the flowing salt will absorb the thermal energy. Another application of molten salt as a working fluid is in a power tower plant. Heliostats are placed around a tower with a receiver. The mirrors are all aimed to the receiver where the molten salt is flowing past in a pipe. Again the molten salt will absorb the thermal energy from the sun.

In both scenarios, the hot molten salt is used to heat water into steam in a Brayton cycle. The Brayton cycle will produce electricity which can be inputted into the electric grid.

Knowledge of the chemistry of the molten salts in question is necessary in both an efficiency sense and a business sense. One of the main goals is to produce a salt with a low melting temperature. Operating a concentrated solar power plant using a working fluid with a low melting temperature will be more efficient than using a similar salt with a higher melting temperature because the plant will use less energy.

In nitrate salt mixtures, eutectic points exist. A eutectic point is where, at a specific chemical composition, the system solidifies at a lower temperature than at any other composition [3]. At the eutectic point, the liquid mixture of the two components is in equilibrium with the crystals of each component. If the temperature is lowered past the eutectic temperature, each component will begin to crystallize out of the mixture [4]. Using a salt with a composition at or near its eutectic composition will have a lower melting temperature than, for instance, using a pure salt. Subsequently, information about the eutectic compositions of different salt systems is desired.

Experimental data exist for some salt systems, mainly binary systems, but not all. Data on ternary systems is also present but not fully known. Differential scanning calorimetry experiments can be conducted to find melting temperatures of salts at different compositions and eventually with enough experimental data, phase diagrams can be constructed. This process can be tedious and costly. Care must be taken to buy and use salts with little impurities, and also to accurately mix salts with the desired concentrations. Testing many different compositions of different salt mixtures will be time consuming. If accurate predictions of salt phase diagrams can

be made instead, the time and money consumed to experimentally produce these phase diagrams can be saved.

This present research puts forward modeling phase diagrams using a Gibbs function minimization technique. The Gibbs function is defined as the difference between the enthalpy and product of the temperature and entropy, as shown below.

$$G = H - TS \tag{1}$$

The Gibbs function, also known as, Gibbs free energy is used to determine whether or not a system is in equilibrium, and the composition at which it will occur. This is used as the basis for the modeling illustrated below.

The structure of this thesis will be as follows. Chapter two will present background literature that was used as a starting point for this work. Chapter three will delve into the methods employed to generate the experimental data against which our models were compared. Chapter four will discuss the mathematical model used to predict the phase diagrams of the nitrate salts studied, and the numerical method that executed this. Chapter five will examine the results of the predictions and will compare these to empirical data. The conclusions of this work will be presented in chapter six, and in chapter seven suggestions for future work will be provided.

Chapter 2. Background Literature

The assertion that molten nitrate salts would be very useful in energy storage systems as well as in solar thermal energy applications as a working fluid is not relatively novel, but has been known for some time [5]. Despite this, there was an admitted lack of information on the properties of these salts [6]. With advancements in differential scanning calorimetry technology and other methods, more experimental data has surfaced [7]. In addition to property data, many attempts to calculate phase diagrams have been purported. This is seen in CALPHAD and other methods [8].

Some of the previous works that have studied the phase diagrams of selected nitrate salts are mentioned below. O.J. Kleppa and L.S. Hersh [6,9] studied the heats of mixing in liquid alkali nitrate salt systems in 1960. More specifically, they studied binary salt systems with nitrate being the common anion. Using a high-temperature reaction calorimeter, measurements of the heats of mixing were taken. Kleppa's empirical values for the heat of mixing data were used a basis for the phase diagram modeling here.

In addition, C.M. Kramer and C.J. Wilson [5] examined the phase diagram of the sodium nitrate-potassium nitrate binary system. Their theoretical derivation, that the solid and liquid solutions of a system are in equilibrium when the free energy is set equal to zero, was used as a starting point for our mathematical model. This was used to study other binary nitrate systems and the more complicated ternary system.

More recently, Xuejan Zhang et al. [10,11] investigated the phase diagrams of the lithium-potassium nitrate and sodium-potassium nitrate systems in 2001 and 2003, respectively. Again, their thermodynamic relationships served as a basis for the modeling here and was in agreement with the relationships observed in previous works.

The experimental data produced by Zhang [10,11], A. N. Campbell et al. [12], and C. Vallet [13], was used as a comparison with the phase diagrams predicted here and also with the experimental data that was produced by our group, which will be discussed in the next section. Their data served as another check to the accuracy of the collection methods of our group and to the phase diagram simulations that were produced.

Data for the lithium-sodium-potassium nitrate ternary salt was limited, and modeling attempts were hard to find. A journal piece by A. G. Bergman and K. Nogoev [14] presents experimental data on the ternary system. This data is once more used a reference for the ternary system modeling and data collection shown here.

The literature above provided a starting ground for the results illustrated here and this present research expands upon these previous works.

Chapter 3. Experimental Methods

Experiments were conducted to determine phase diagrams of the salt mixtures investigated in this present work. Research engineers from Dynalene Inc., an industrial heat transfer fluid manufacturer, teamed up with students and faculty from Lehigh University to study nitrate salts. The research included determining the properties of these salts and the modeling of their phase diagrams. The results of the present calculations have been compared with the experiments conducted at Dynalene [15,16]. A discussion of these experiments is provided here.

Using the equipment and resources at Dynalene Inc., the experiments were made possible. Differential scanning calorimetry (DSC) was used to determine the phase diagrams of the salt mixtures. DSC is a measuring technique used to determine temperatures as well as heat flows during phase changes, such as melting or crystallization [7]. The differential scanning calorimeter used here was the TA DSC Q200. Because of the temperature limitations of the machine, isothermal runs were only performed to 400°C. Phase transitions were calibrated using high purity indium.

The salts used were American Chemical Society (ACS) grade lithium, sodium, and potassium nitrate. These salts were dried in a furnace at 150°C for 24 hours and stored over a desiccant to ensure purity. The dried salts were measure out using a Mettler-Toledo XS-205 analytical balance which carried out masses to ±0.001 grams; this guaranteed the accuracy of the ratio of the salts being measured.

After measurement, the binary mixtures were placed in a furnace to fuse at 350°C for at least 24 hours, to obtain sufficient homogenization. Ternary mixtures were kept there for 48 hours to ensure uniformity due to the addition of the third component. The experimenter notes that exposing the salts to these temperatures for that period of time did not initiate thermal

degradation based on evidence from previous experiments and reports from literature. Each salt mixture was tested by the DSC three times, with more runs performed for mixtures close to the suspected eutectic composition.

The framework of each salt sample was established by using a heating rate of 10°C/min to provide a general idea of where to look for the solidus and liquidus points on the DSC plot. Melting runs were carried out to 320°C and then cooled to the original holding temperature at a rate of 5°C/min. Upon heating, the solidus for each plot is defined as the first deviation from the baseline and the liquidus is defined as the largest signal of the last thermal event prior to its return to the baseline. Upon cooling, the liquidus is defined as the first deviation from the baseline and the solidus is the deviation from the last thermal event prior to returning to the baseline.

Chapter 4. Mathematical Model

4.1 Binary Formulation

Modeling a binary system, begins with setting the Gibbs free energy of the system equal to zero [5]. In a system with two components, A and B, this is done for each component. The free energy consists of three terms: first, the fusion term, second, the free energy of mixing of the liquid solution, and finally the free energy of mixing of the solid solution. Because the free energy is set to zero, both the liquid and solid solutions of each component are in thermodynamic equilibrium. For example, the free energy of component A is expressed as

$$\Delta G^{A}=(\Delta H_{A}-T\Delta S_{A})+(\Delta H_{mix}^{Al}-T\Delta S_{mix}^{Al})-(\Delta H_{mix}^{As}-T\Delta S_{mix}^{As}) \quad (2)$$

where, as described above, it is seen split into three terms [5].

Expanding the components of the first term leads to

$$\Delta H_{A}=\Delta H_{fus}^{A}-\int_{T}^{Tmp}(C_{Pl}-C_{Ps})dT \quad (3)$$

and

$$\Delta S_{A}=\Delta S_{fus}^{A}-\int_{T}^{Tmp}\frac{(C_{Pl}-C_{Ps})}{T}dT \quad (4)$$

where ΔH_{fus}^{A} and ΔS_{fus}^{A} are the enthalpy and entropy of fusion of component A, respectively, at its melting point. To account for the temperature difference between the salt's current temperature and its melting temperature, a correction term is needed. The correction terms use the difference in specific heat between the liquid (C_{Pl}) and solid (C_{Ps}) phases. The correction terms are integrated over the temperature range, starting from the component's melting temperature to the current temperature at which the equation is being solved. Integration of the enthalpy equation leads to

$$\Delta H_{A}=\Delta H_{fus}^{A}-\Delta C_{PA}(T_{mp}^{A}-T) \quad (5)$$

where ΔC_{PA} is used to denote the difference between C_{Pl} and C_{Ps}. The melting temperature of the component is represented as T_{mp}^{A} and T is the current temperature of the system. Next, the equation below is used to relate the entropy of fusion to the enthalpy of fusion of component A.

$$\Delta S_{fus}^{A} = \frac{\Delta H_{fus}^{A}}{T_{mp}^{A}} \tag{6}$$

Integration of the entropy equation and application of the above substitution for ΔS_{fus}^{A} leads to

$$\Delta S_{A} = \frac{\Delta H_{fus}^{A}}{T_{mp}^{A}} - \Delta C_{PA}\left(ln\frac{T_{mp}^{A}}{T}\right) \tag{7}$$

Now that the terms ΔH_A and ΔS_A have been expanded, these expressions can be plugged into the first term of the Gibbs free energy equation, shown below.

$$\Delta H_A - T\Delta S_A = \Delta H_{fus}^{A} - \Delta C_{PA}\left(T_{mp}^{A} - T\right) - T\left[\frac{\Delta H_{fus}^{A}}{T_{mp}^{A}} - \Delta C_{PA}\left(ln\frac{T_{mp}^{A}}{T}\right)\right] \tag{8}$$

Rearranging this equation and it becomes,

$$\Delta H_A - T\Delta S_A = \left(1 - \frac{T}{T_{mp}^{A}}\right)\Delta H_{fus}^{A} + \Delta C_{PA}\left[T - T_{mp}^{A} - T\,ln\frac{T}{T_{mp}^{A}}\right] \tag{9}$$

The Gibbs-Duhem equation must be utilized to determine ΔH_{mix}^{A} in both the liquid and solid phases [5]. The Gibbs-Duhem equation, for component A, is defined as follows

$$\Delta H_{mix}^{A} = \Delta H_{mix} + (1 - x_A)\frac{d\Delta H_{mix}}{dx_A} \tag{10}$$

where, the enthalpy of mixing, ΔH_{mix}, in its most general manner, is expressed as a polynomial of the form

$$\Delta H_{mix} = x_A x_B (a + b x_A + c x_A x_B) \tag{11}$$

Here x_A and x_B are the mole fractions of each component with x_A as the component with the smaller cation. The letters *a, b,* and *c* represent empirical coefficients. Determination of these coefficients is discussed later. The second term in the Gibbs-Duhem equation, shown above, is the product of $(1\text{-}x_A)$ and the total derivative of the enthalpy of mixing, ΔH_{mix}, taken with

respect to x_A. Taking the derivative correctly (with respect to x_A) requires that $(1\text{-}x_A)$ is substituted in for each x_B. This is done because x_B is related to x_A and this effect must be taken into account. Applying this substitution and then taking the derivative results in

$$\frac{d\Delta H_{mix}}{dx_A} = -ax_A + ax_B - bx_A^2 + 2bx_Ax_B - 2cx_A^2x_B + 2cx_Ax_B^2 \quad (12)$$

Plugging this derivative into the Gibbs-Duhem equation, and after cancelling of like terms, the partial molar enthalpy of mixing for component A becomes,

$$\Delta H_{mix}^A = ax_B^2 + 2bx_Ax_B^2 + 2cx_Ax_B^3 - cx_A^2x_B^2 \quad (13)$$

This same procedure is applied to each phase, both the liquid and the solid. To determine the partial molar enthalpy of mixing for component B, the Gibbs-Duhem equation is again used, this time of the form

$$\Delta H_{mix}^B = \Delta H_{mix} + (1\text{-}x_B)\frac{d\Delta H_{mix}}{dx_B} \quad (14)$$

Expanding this term is accomplished in the same manner as it was for component A.

The partial molar entropy of mixing in the liquid and solid phases for component A becomes

$$\Delta S_{mix}^A = -R \ln x_A \quad (15)$$

where x_A is either the mole fraction of component A on the liquidus curve for the liquid phase or the mole fraction of A on the solidus curve for the solid phase. *R* represents the universal gas constant. Similarly, for component B, the expression becomes,

$$\Delta S_{mix}^B = -R \ln x_B \quad (16)$$

Again, x_B is the mole fraction of component B either on the liquidus or solidus curve depending on the phase. This is the expression because the mixture is assumed to be a regular solution [5].

Combining the above terms produces the Gibbs free energy for a component. For component A, this becomes

$$\Delta G^A = \left(1 - \frac{T}{T_{mp}^A}\right)\Delta H_{fus}^A + \Delta C_{PA}\left[T - T_{mp}^A - T\,ln\frac{T}{T_{mp}^A}\right] + RT\left(ln\,x_A^l - ln\,x_A^s\right) + \left(a_l x_B^2 + 2b_l x_A x_B^2 + 2c_l x_A x_B^3 - c_l x_A^2 x_B^2\right) - \left(a_s x_B^2 + 2b_s x_A x_B^2 + 2c_s x_A x_B^3 - c_s x_A^2 x_B^2\right) \quad (17)$$

where empirical coefficients with the *l* and *s* subscripts are from the liquid and solid enthalpies of mixing respectively. A similar equation can be developed for component B.

Currently, there are only two equations for five unknowns, $x_A^l, x_B^l, x_A^s, x_B^s$ and T. Two more equations come from the relation between the concentrations of the components in each phase. They are related as follows

$$x_A^l + x_B^l = 1 \quad (18)$$

$$x_A^s + x_B^s = 1 \quad (19)$$

where the *l* and *s* represent the liquid and solid phase, respectively. There is still one more unknown than there are equations. In order to solve the four equations, one of the unknowns must be given. When one of these is known, the four equations are solved simultaneously at each composition (or temperature) to produce the phase diagrams.

4.2 Coefficients

Empirical coefficients are needed to properly represent the partial molar enthalpies of mixing for both the solid and liquid phases. Kleppa [6] was able to experimentally derive the expressions and coefficients for the enthalpy of mixing for various binary mixtures. He conducted mixing experiments of different alkali nitrate salts and using the least squares method, he was able to determine values for the empirical coefficients of the enthalpy of mixing for the liquid phase. These values provided the basis for coefficients used in the present work.

Specifically, his data for the $NaNO_3$- KNO_3, $LiNO_3$-$NaNO_3$, and $LiNO_3$- KNO_3 binary systems was used.

Kleppa though, did not provide values for the coefficients of the enthalpy of mixing for the solid phase. Kramer [5], in his 1980's paper on the $NaNO_3$- KNO_3 system, modeled the binary salt and did give an expression for the enthalpy of mixing for the solid phase. This was used as the expression for the solid phase enthalpy of mixing here, but also as a base value for the other two binary systems.

In order to more accurately match the phase diagram simulations to the experimental data that was obtained, slight changes to some of Kleppa's liquid coefficients were made. Changes in the values of the coefficients had some predictable effects on the phase diagram's shape. A change in the magnitude of the 'a' coefficient caused the eutectic point to be shifted either up or down in temperature. Increasing it, decreased the eutectic temperature, while decreasing the magnitude increased the eutectic temperature. The magnitude of the 'b' coefficient affects the symmetry of the liquidus curve around the eutectic point. So, increasing (decreasing) this magnitude shifts the eutectic to the left (right) on a phase diagram, resulting in a different concentration being the eutectic concentration. And the addition of the 'c' coefficient is needed when there is a large temperature difference between the pure salt's melting temperature and the eutectic temperature. It ensures that the modeling will be more accurate. The 'c' coefficient is present in the $LiNO_3$- KNO_3 enthalpy of mixing expression, because for this phase diagram a change in the composition has a larger effect on the corresponding temperature compared to the other two binary systems.

It should also be noted that results described above were the main effect observed by the changes in the coefficients, but by no means were they the only effects identified. While a

change in the 'a' coefficient did predominantly effect the temperature of the eutectic, it did to some extent also change the composition. Likewise, a modification of the 'b' coefficient did slightly effect the eutectic temperature in addition to primarily changing the eutectic composition.

The solid coefficients of the enthalpy of mixing were chosen accordingly to, as expected, agree with the experimental data. Some observations were made when choosing the solid coefficients as well. Drastic changes in the value of the solid coefficients did have some effect on the shape of liquidus curves and the location of the eutectic, while changes in the value of the liquid coefficients had only marginal effects on the solidus curves. In addition, changes in the 'a' coefficient only, or the 'b' coefficient only, had a similar effect on the solidus curves. Hence, changes in the solid coefficients had a combined effect; the larger the magnitude of these coefficients and the solidus curves were shifted outward towards the pure component's composition, and had much steeper slopes. Conversely, smaller magnitudes resulted in curves that bent in toward the eutectic point with shallower slopes. This effect can be seen in the phase diagram below.

An example of the $LiNO_3$-$NaNO_3$ phase diagram is shown. Three different sets of solid enthalpy of mixing coefficients were used while the liquid empirical coefficients were kept constant. The first set, graphed as 'Coefficients 1' has intermediate values of the 'a' and 'b' coefficients, being 9204.8 and 3347.2 joules per mole respectively. The second set, graphed as 'Coefficients 2', was produced from 'a' equal to 12,552 joules per mole and 'b' equal to 6276 joules per mole. Compared to 'Coefficients 1', 'Coefficients 2' contains solidus curves which are very vertical and do not bend in towards the eutectic point at all. In addition, the resulting

eutectic point is both slightly lowered and shifted to the right as a result of the change in coefficients.

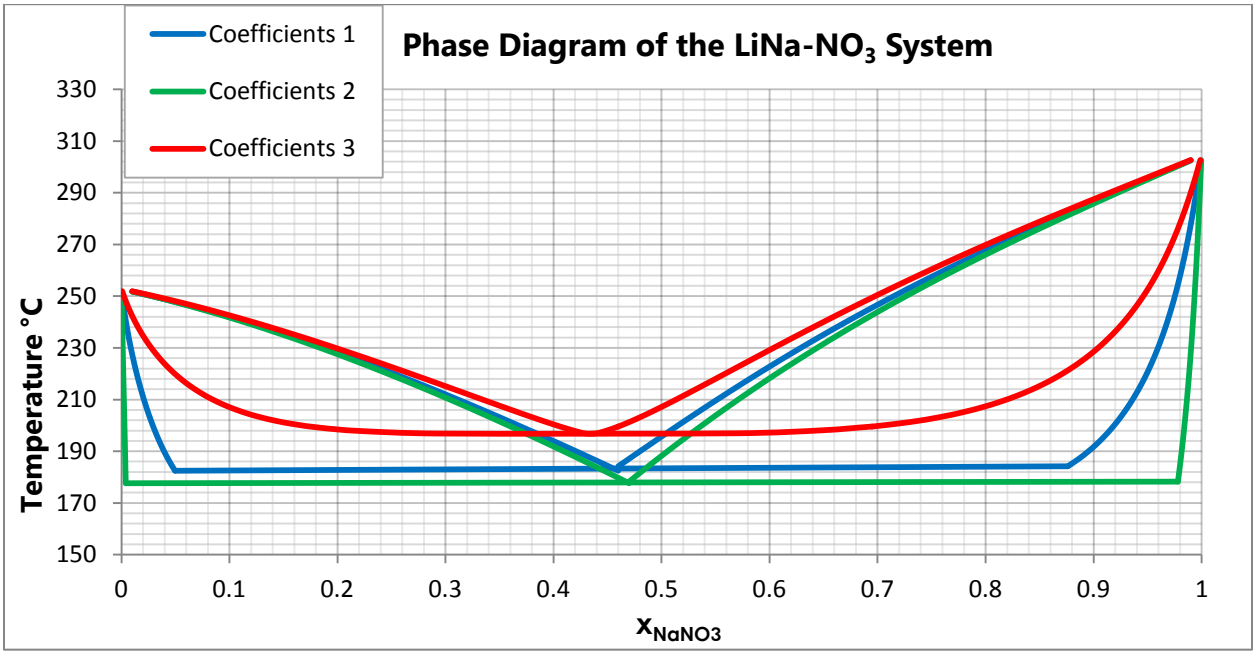

Figure 1. Effect of solid enthalpy of mixing coefficient values on phase diagram shape

Now, comparing 'Coefficients 3' to 'Coefficients 1', the opposite effects are apparent. 'Coefficients 3' uses values of 'a' and 'b' equal to 6276 and 2092 joules per mole, respectively, must lower than those used in 'Coefficients 1' . The solidus curves produced from these coefficients have much shallower slopes and curve in all the way to meet at the eutectic point. Again, the location of the eutectic point was altered; the new location had a higher temperature and lower composition of $NaNO_3$. The enthalpy of mixing coefficients for the solid phase were chosen accordingly to match the experimental data our group collected.

Now that the determination of the coefficients has been discussed, the ternary formulation will now be presented.

4.3 Ternary Formulation

In a ternary system of nitrate salts, the Gibbs free energy of each component is set equal to zero. Again, as in a binary system, the solid and liquid phases of each component are in thermodynamic equilibrium, and each component is in equilibrium with the other. At each composition of the salt, there are five equations that need to be satisfied. First, the free energy of all three components must be fulfilled, and then the relation between the component's compositions in the both liquid and solid phases provide the last two equations. Consequently, there are seven unknowns and only five equations. Therefore, the compositions of two of the components must be known. Solving these five equations simultaneously provides solutions for the liquid and solid compositions for each component and the temperature at these compositions.

As in a binary system, the free energy of a component A, for example, becomes,

$$\Delta G^{A}=(\Delta H_{A}-T\Delta S_{A})+(\Delta H_{mix}^{Al}-T\Delta S_{mix}^{Al})-(\Delta H_{mix}^{As}-T\Delta S_{mix}^{As}) \quad (20)$$

and the same expressions exist for the other two components. Expansion of each of these terms is completed using the same approach to that of the binary system. Determining the partial enthalpy of mixing for each component is a bit more complex. The enthalpy of mixing for the ternary system is expressed as the addition of the three binary mixing interactions. The ternary interaction of the three components is assumed to be negligible compared to the binary interactions and is therefore omitted. Further research can be conducted into the ternary interaction to validate this claim. Expansion of the enthalpy of mixing of the liquid phase for the ternary system is shown below. The form used is

$$G_{mix}^{liq} = G_{NaK}^{E} + G_{LiK}^{E} + G_{LiNa}^{E} \quad (21)$$

where G^{E} is equivalent to ΔH_{mix} as seen in the binary formulation. This is expanded as

$$G_{mix}^{liq} = (a_1 x_a x_b + b_1 x_a^2 x_b) + (a_2 x_b x_c + b_2 x_b x_c^2 + c_2 x_b^2 x_c^2) + (a_3 x_a x_c + b_3 x_a x_c^2) \quad (22)$$

where x_a, x_b, and x_c represent the liquid concentrations of $NaNO_3$, KNO_3, and $LiNO_3$ respectively. The coefficients here are those from the three binary systems. The presence of the *c* coefficient in the $LiNO_3$-KNO_3 expressions and not the others is due to the large temperature difference between the eutectic and the pure component's melting temperatures. Again, the Gibbs-Duhem equation must be applied to determine the partial molar enthalpy of mixing for each component. For component A, the form of the equation used is shown below

$$G_{mix}^{A} = G_{mix}^{liq} + (1 - x_a)\frac{\partial G^{liq}}{\partial x_a} \tag{23}$$

For this equation to be valid, the ratio of the two other liquid concentrations must be kept constant. This ratio will be known as *C*, as seen below

$$\frac{x_b}{x_c} = C \tag{24}$$

This must be done to ensure that when taking the partial derivative, that the effects of the other components are kept constant. Here $\frac{\partial G^{liq}}{\partial x_a}$ is the partial derivative of G_{mix}^{liq} taken with respect to component A. The differentiation is illustrated here,

$$G_{mix}^{A} = G_{mix}^{liq} + (1 - x_a)[a_1 x_a \frac{\partial x_b}{\partial x_a} + a_1 x_b + b_1 x_a^2 \frac{\partial x_b}{\partial x_a} + 2b_1 x_a x_b + a_2 x_b \frac{\partial x_c}{\partial x_a} + a_2 x_c \frac{\partial x_b}{\partial x_a} +$$

$$2b_2 x_b x_c \frac{\partial x_c}{\partial x_a} + b_2 x_c^2 \frac{\partial x_b}{\partial x_a} + 2c_2 x_b^2 x_c \frac{\partial x_c}{\partial x_a} + 2c_2 x_b x_c^2 \frac{\partial x_b}{\partial x_a} + a_3 x_a \frac{\partial x_c}{\partial x_a} + a_3 x_c + 2b_3 x_a x_c \frac{\partial x_c}{\partial x_a} +$$

$$b_3 x_c^2] \tag{25}$$

Combining like terms,

$$G_{mix}^{A} = G_{mix}^{liq} + (1 - x_a)[a_1 x_b + 2b_1 x_a x_b + a_3 x_c + b_3 x_c^2 + \frac{\partial x_b}{\partial x_a}(a_1 x_a + b_1 x_a^2 + a_2 x_c + b_2 x_c^2 +$$

$$2c_2 x_b x_c^2) + \frac{\partial x_c}{\partial x_a}(a_2 x_b + 2b_2 x_b x_c + a_3 x_a + 2b_3 x_a x_c + 2c_2 x_b^2 x_c)] \tag{26}$$

Next, the terms $\frac{\partial x_b}{\partial x_a}$ and $\frac{\partial x_c}{\partial x_a}$ must be evaluated and expressed in terms of the concentrations. To do this, the equation below is utilized.

$$x_A + x_B + x_C = 1 \tag{27}$$

The substitution $x_C = \frac{x_B}{C}$ is used for x_C and after rearranging, the equation becomes,

$$x_B\left(1 + \frac{1}{C}\right) = 1 - x_A \tag{28}$$

Dividing both sides by the value $\left(1 + \frac{1}{C}\right)$ and it produces

$$x_B = \frac{1-x_A}{\left(1+\frac{1}{C}\right)} \tag{29}$$

After differentiation with respect to component A, and substituting back in for C

$$\frac{\partial x_b}{\partial x_a} = \frac{-1}{\left(1+\frac{x_c}{x_b}\right)} \tag{30}$$

And finally, rearranging the right side of the equation and substituting, $1 - x_A$ for $x_B + x_C$ the equation becomes

$$\frac{\partial x_B}{\partial x_A} = \frac{-x_B}{(1-x_A)} \tag{31}$$

A similar procedure is followed to determine $\frac{\partial x_c}{\partial x_a}$. Again, starting with the equation below, but now utilizing the substitution $x_B = Cx_C$.

$$x_A + x_B + x_C = 1 \tag{32}$$

Substituting and rearranging,

$$x_C(1 + C) = 1 - x_A \tag{33}$$

Dividing both sides by the value $(1 + C)$ and it produces

$$x_C = \frac{1-x_A}{(1+C)} \tag{34}$$

After differentiation with respect to component B, and substituting back in for C

$$\frac{\partial x_C}{\partial x_A} = \frac{-1}{\left(1+\frac{x_B}{x_C}\right)} \tag{35}$$

And again, rearranging the right side of the equation and substituting, $1 - x_A$ for $x_B + x_C$ the equation becomes

$$\frac{\partial x_C}{\partial x_A} = \frac{-x_C}{(1-x_A)} \tag{36}$$

These two results are now substituted into the enthalpy of mixing equation as seen below.

$$G_{mix}^{A} = G_{mix}^{liq} + (1 - x_a)[a_1 x_b + 2b_1 x_a x_b + a_3 x_c + b_3 x_c^2 + \frac{-x_b}{1-x_a}(a_1 x_a + b_1 x_a^2 + a_2 x_c +$$

$$b_2 x_c^2 + 2c_2 x_b x_c^2) + \frac{-x_c}{1-x_a}(a_2 x_b + 2b_2 x_b x_c + a_3 x_a + 2b_3 x_a x_c + 2c_2 x_b^2 x_c)] \tag{37}$$

Simplifying,

$$G_{mix}^{A} = G_{mix}^{liq} + (1 - x_a)[a_1 x_b + 2b_1 x_a x_b + a_3 x_c + b_3 x_c^2] - x_b(a_1 x_a + b_1 x_a^2 + a_2 x_c + b_2 x_c^2 +$$

$$2c_2 x_b x_c^2) - x_c(a_2 x_b + 2b_2 x_b x_c + a_3 x_a + 2b_3 x_a x_c + 2c_2 x_b^2 x_c) \tag{38}$$

Now substituting in for G_{mix}^{liq} and again simplifying,

$$G_{mix}^{A} = (a_1 x_a x_b + b_1 x_a^2 x_b) + (a_2 x_b x_c + b_2 x_b x_c^2 + c_2 x_b^2 x_c^2) + (a_3 x_a x_c + b_3 x_a x_c^2) +$$

$$(1 - x_a)[a_1 x_b + 2b_1 x_a x_b + a_3 x_c + b_3 x_c^2] - a_1 x_a x_b - b_1 x_a^2 x_b - a_2 x_b x_c - b_2 x_b x_c^2 -$$

$$a_2 x_b x_c - 2b_2 x_b x_c^2 - a_3 x_a x_c - 2b_3 x_a x_c^2 - 2c_2 x_b^2 x_c^2 - 2c_2 x_b^2 x_c^2 \tag{39}$$

And finally, after crossing out like terms the final form the partial enthalpy of mixing for component A is produced,

$$G_{mix}^{A} = (1 - x_a)[a_1 x_b + 2b_1 x_a x_b + a_3 x_c + b_3 x_c^2] - a_2 x_b x_c - 2b_2 x_b x_c^2 - b_3 x_a x_c^2 - 3c_2 x_b^2 x_c^2$$

(40)

This same method is used for components B and C. For component B, the form of the Gibbs-Duhem equation that is used is

$$G_{mix}^{B} = G_{mix}^{liq} + (1 - x_b)\frac{\partial G^{liq}}{\partial x_b} \tag{41}$$

where now, the ratio between the liquid concentrations of components A and C is held constant as seen below,

$$\frac{x_A}{x_C} = C \tag{42}$$

Here $\frac{\partial G^{liq}}{\partial x_B}$ is the partial derivative of G_{mix}^{liq} taken with respect to component B. The differentiation is illustrated here,

$$G_{mix}^{B} = G_{mix}^{liq} + (1 - x_b)[a_1 x_b \frac{\partial x_a}{\partial x_b} + a_1 x_a + b_1 x_a^2 + 2b_1 x_a x_b \frac{\partial x_a}{\partial x_b} + a_2 x_b \frac{\partial x_c}{\partial x_b} + a_2 x_c +$$

$$2b_2 x_b x_c \frac{\partial x_c}{\partial x_b} + b_2 x_c^2 + 2c_2 x_b^2 x_c \frac{\partial x_c}{\partial x_b} + 2c_2 x_b x_c^2 + a_3 x_a \frac{\partial x_c}{\partial x_b} + a_3 x_c \frac{\partial x_a}{\partial x_b} + 2b_3 x_a x_c \frac{\partial x_c}{\partial x_b} +$$

$$b_3 x_c^2 \frac{\partial x_a}{\partial x_b}] \tag{43}$$

After rearranging like terms together,

$$G_{mix}^{B} = G_{mix}^{liq} + (1 - x_b)[a_1 x_a + b_1 x_a^2 + a_2 x_c + b_2 x_c^2 + 2c_2 x_b x_c^2 + \frac{\partial x_c}{\partial x_b}(a_2 x_b + 2b_2 x_b x_c +$$

$$2c_2 x_b^2 x_c + a_3 x_a + 2b_3 x_a x_c) + \frac{\partial x_a}{\partial x_b}(a_1 x_b + 2b_1 x_a x_b + a_3 x_a + b_3 x_c^2)] \tag{44}$$

Again, the terms $\frac{\partial x_A}{\partial x_B}$ and $\frac{\partial x_C}{\partial x_B}$ must be evaluated and expressed in terms of the concentrations. This process is the same as it was for component A, as demonstrated above. The final forms for each term are

$$\frac{\partial x_A}{\partial x_B} = \frac{-x_A}{1-x_B} \tag{45}$$

and

$$\frac{\partial x_C}{\partial x_B} = \frac{-x_C}{1-x_B} \tag{46}$$

Plugging these into the equation above, and after simplifying,

$$G_{mix}^{B} = G_{mix}^{liq} + (1 - x_b)[a_1 x_a + b_1 x_a^2 + a_2 x_c + b_2 x_c^2 + 2c_2 x_b x_c^2] - x_c(a_2 x_b + 2b_2 x_b x_c +$$

$$2c_2 x_b^2 x_c + a_3 x_a + 2b_3 x_a x_c) - x_a(a_1 x_b + 2b_1 x_a x_b + a_3 x_a + b_3 x_c^2) \tag{47}$$

And finally, after plugging in G_{mix}^{liq} and simplifying, the result for the partial molar enthalpy of mixing for component B becomes,

$$G_{mix}^{B} = (1 - x_b)[a_1 x_a + b_1 x_a^2 + a_2 x_c + b_2 x_c^2 + 2c_2 x_b x_c^2] - b_1 x_a^2 x_b - b_2 x_b x_c^2 - c_2 x_b^2 x_c^2 - 2b_3 x_a x_c^2 - a_3 x_a x_c \quad (48)$$

On to component C, where the form of the Gibbs-Duhem equation is now

$$G_{mix}^{C} = G_{mix}^{liq} + (1 - x_c)\frac{\partial G^{liq}}{\partial x_c} \quad (49)$$

where the constant *C* is now equal to the ratio between the liquid concentrations of components A and B,

$$\frac{x_A}{x_B} = C \quad (50)$$

After differentiation,

$$G_{mix}^{C} = G_{mix}^{liq} + (1 - x_c)[a_1 x_a \frac{\partial x_b}{\partial x_c} + a_1 x_b \frac{\partial x_a}{\partial x_c} + b_1 x_a^2 \frac{\partial x_b}{\partial x_c} + 2b_1 x_a x_b \frac{\partial x_a}{\partial x_c} + a_2 x_b + a_2 x_c \frac{\partial x_b}{\partial x_c} + 2b_2 x_b x_c + b_2 x_c^2 \frac{\partial x_b}{\partial x_c} + 2c_2 x_b^2 x_c + 2c_2 x_b x_c^2 \frac{\partial x_b}{\partial x_c} + a_3 x_a + a_3 x_c \frac{\partial x_a}{\partial x_c} + 2b_3 x_a x_c + b_3 x_c^2 \frac{\partial x_a}{\partial x_c}] \quad (51)$$

The two terms $\frac{\partial x_A}{\partial x_C}$ and $\frac{\partial x_B}{\partial x_C}$ must again be expressed in terms of the component's concentrations. Again, this process is the same as it was for component A, and is demonstrated above. The final forms for each term become,

$$\frac{\partial x_A}{\partial x_C} = \frac{-x_A}{1 - x_C} \quad (52)$$

and

$$\frac{\partial x_B}{\partial x_C} = \frac{-x_B}{1 - x_C} \quad (53)$$

Now, using these two terms and after some simplification,

$$G_{mix}^{C} = G_{mix}^{liq} + (1 - x_c)[a_2 x_b + 2b_2 x_b x_c + 2c_2 x_b^2 x_c + a_3 x_a + 2b_3 x_a x_c] - x_a(a_1 x_b + 2b_1 x_a x_b + a_3 x_c + b_3 x_c^2) - x_b(a_1 x_a + b_1 x_a^2 + a_2 x_c + b_2 x_c^2 + 2c_2 x_b x_c^2) \quad (54)$$

Plugging in for G_{mix}^{liq} and after more simplification, the final form for the partial molar enthalpy of mixing for component C is obtained,

$$G_{mix}^{C} = (1 - x_c)[a_2 x_b + 2b_2 x_b x_c + 2c_2 x_b^2 x_c + a_3 x_a + 2b_3 x_a x_c] - a_1 x_a x_b - 2b_1 x_a^2 x_b - c_2 x_b^2 x_c^2 \quad (55)$$

The above derivations were for the partial enthalpy of mixing in the liquid phase. Determining the partial enthalpy of mixing for the solid phase is accomplished in a similar fashion and is shown here. Component A will be the concentration of $NaNO_3$, component B is KNO_3, and component C is $LiNO_3$. These concentrations are all of the solid phase. The form of the enthalpy of mixing for the solid phase is shown below.

$$G_{mix}^{sol} = G_{NaK}^{E} + G_{LiK}^{E} + G_{LiNa}^{E} \quad (56)$$

Again, it is the addition of the three binary interactions. Expansion of this leads to

$$G_{mix}^{sol} = (a_1 x_a x_b) + (a_2 x_b x_c + b_2 x_b x_c^2) + (a_3 x_a x_c + b_3 x_a x_c^2) \quad (57)$$

where these coefficients are those from the enthalpy of mixing in the solid phase of the three binary systems. Determining the partial molar enthalpy of mixing for each component again involves employing the Gibbs-Duhem equation. For component A,

$$G_{mix}^{A} = G_{mix}^{sol} + (1 - x_a)\frac{\partial G^{sol}}{\partial x_a} \quad (58)$$

where $\frac{\partial G^{sol}}{\partial x_a}$ is the partial derivative of the solid enthalpy of mixing expression above, taken with respect to component A. As with the liquid phase, the ratio of the concentrations of components B and C have to be kept constant during this differentiation as seen below,

$$\frac{x_B}{x_C} = C \quad (59)$$

Following differentiation,

$$G_{mix}^{A} = G_{mix}^{sol} + (1 - x_a)[a_1 x_a \frac{\partial x_b}{\partial x_a} + a_1 x_b + a_2 x_b \frac{\partial x_c}{\partial x_a} + a_2 x_c \frac{\partial x_b}{\partial x_a} + 2b_2 x_b x_c \frac{\partial x_c}{\partial x_a} + b_2 x_c^2 \frac{\partial x_b}{\partial x_a} + a_3 x_a \frac{\partial x_c}{\partial x_a} + a_3 x_c + 2b_3 x_a x_c \frac{\partial x_c}{\partial x_a} + b_3 x_c^2] \quad (60)$$

The terms $\frac{\partial x_B}{\partial x_A}$ and $\frac{\partial x_C}{\partial x_A}$ again need to be expanded, and the expansions are exactly the same as they are for component A in the liquid solution, are reproduced below.

$$\frac{\partial x_B}{\partial x_A} = \frac{-x_b}{1-x_a} \tag{61}$$

$$\frac{\partial x_C}{\partial x_A} = \frac{-x_c}{1-x_a} \tag{62}$$

Rearranging and substituting in the above equations,

$$G_{mix}^{A} = G_{mix}^{sol} + (1-x_a)[a_1x_b + a_3x_c + b_3x_c^2 + \frac{-x_b}{1-x_a}(a_1x_a + a_2x_c + b_2x_c^2) + \frac{-x_c}{1-x_a}(a_2x_b + 2b_2x_bx_c + a_3x_a + 2b_3x_ax_c)] \tag{63}$$

Simplifying and substituting in for G_{mix}^{sol},

$$G_{mix}^{A} = (a_1x_ax_b) + (a_2x_bx_c + b_2x_bx_c^2) + (a_3x_ax_c + b_3x_ax_c^2) + (1-x_a)[a_1x_b + a_3x_c + b_3x_c^2] - a_1x_ax_b - a_2x_bx_c - b_2x_bx_c^2 - a_2x_bx_c - 2b_2x_bx_c^2 - a_3x_ax_c - 2b_3x_ax_c^2 \tag{64}$$

And finally canceling out like terms, the final form for component A is,

$$G_{mix}^{A} = (1-x_a)[a_1x_b + a_3x_c + b_3x_c^2] - a_2x_bx_c - 2b_2x_bx_c^2 - b_3x_ax_c^2$$

Again for component B, the Gibbs-Duhem equation becomes,

$$G_{mix}^{B} = G_{mix}^{sol} + (1-x_b)\frac{\partial G^{sol}}{\partial x_b} \tag{65}$$

where the ratio between the concentrations of components A and C is kept constant.

Differentiating and the expression becomes,

$$G_{mix}^{B} = G_{mix}^{sol} + (1-x_b)[a_1x_a + a_1x_b\frac{\partial x_a}{\partial x_b} + a_2x_b\frac{\partial x_c}{\partial x_b} + a_2x_c + 2b_2x_bx_c\frac{\partial x_c}{\partial x_b} + b_2x_c^2 + a_3x_a\frac{\partial x_c}{\partial x_b} + a_3x_c\frac{\partial x_a}{\partial x_b} + 2b_3x_ax_c\frac{\partial x_c}{\partial x_b} + b_3x_c^2\frac{\partial x_a}{\partial x_b}] \tag{66}$$

The substitutions for $\frac{\partial x_a}{\partial x_b}$ and $\frac{\partial x_c}{\partial x_b}$ again are the same as that for component B in the liquid phase, seen below

$$\frac{\partial x_A}{\partial x_B} = \frac{-x_b}{1-x_a} \tag{67}$$

$$\frac{\partial x_C}{\partial x_A} = \frac{-x_c}{1-x_a} \tag{68}$$

Applying this substitution and simplifying,

$$G_{mix}^{B} = G_{mix}^{sol} + (1 - x_b)[a_1 x_a + a_2 x_c + b_2 x_c^2] - x_a(a_1 x_b + a_3 x_c + b_3 x_c^2) - x_c(a_2 x_b + 2b_2 x_b x_c + a_3 x_a + 2b_3 x_a x_c) \tag{69}$$

Finally, after substitution for G_{mix}^{sol} and canceling out like terms the expression becomes,

$$G_{mix}^{B} = (1 - x_b)[a_1 x_a + a_2 x_c + b_2 x_c^2] - b_2 x_b x_c^2 - a_3 x_a x_c - 2b_3 x_a x_c^2 \tag{70}$$

And lastly, for component C, the Gibbs-Duhem equation is of the form,

$$G_{mix}^{C} = G_{mix}^{sol} + (1 - x_c)\frac{\partial G^{sol}}{\partial x_c} \tag{71}$$

with the ratio of component A to component B being kept constant. Following differentiation,

$$G_{mix}^{C} = G_{mix}^{sol} + (1 - x_c)[a_1 x_a \frac{\partial x_b}{\partial x_c} + a_1 x_b \frac{\partial x_a}{\partial x_c} + a_2 x_b + a_2 x_c \frac{\partial x_b}{\partial x_c} + 2b_2 x_b x_c + b_2 x_c^2 \frac{\partial x_b}{\partial x_c} + a_3 x_a + a_3 x_c \frac{\partial x_a}{\partial x_c} + 2b_3 x_a x_c + b_3 x_c^2 \frac{\partial x_a}{\partial x_c}] \tag{72}$$

Again the expressions (which are the same as those for component C in the liquid solution) below are used,

$$\frac{\partial x_A}{\partial x_C} = \frac{-x_A}{1-x_C} \tag{73}$$

$$\frac{\partial x_B}{\partial x_C} = \frac{-x_B}{1-x_C} \tag{74}$$

After substitution and rearrangement,

$$G_{mix}^{C} = G_{mix}^{sol} + (1 - x_c)[a_2 x_b + 2b_2 x_b x_c + a_3 x_a + 2b_3 x_a x_c] - x_a(a_1 x_b + a_3 x_c + b_3 x_c^2) - x_b(a_1 x_a + a_2 x_c + b_2 x_c^2)] \tag{75}$$

And finally, after the substitution for G_{mix}^{sol} and simplifying, the final form for the enthalpy of mixing of the solid solution for component C becomes,

$$G_{mix}^{C} = (1 - x_c)[a_2 x_b + 2b_2 x_b x_c + a_3 x_a + 2b_3 x_a x_c] - a_1 x_a x_b \quad (76)$$

Now that each of the terms for the Gibbs free energy for each component have been expanded, they are put together. For component A,

$$\Delta G^A = \left(1 - \frac{T}{T_{mp}^A}\right)\Delta H_{fus}^A + \Delta C_{PA}\left[T - T_{mp}^A - T\,ln\frac{T}{T_{mp}^A}\right] + RT\left(ln\,x_A^l - ln\,x_A^s\right) + \left((1 - x_a)[a_1 x_b + 2b_1 x_a x_b + a_3 x_c + b_3 x_c^2] - a_2 x_b x_c - 2b_2 x_b x_c^2 - b_3 x_a x_c^2 - 3c_2 x_b^2 x_c^2\right) - \left((1 - x_a)[a_1 x_b + a_3 x_c + b_3 x_c^2] - a_2 x_b x_c - 2b_2 x_b x_c^2 - b_3 x_a x_c^2\right) \quad (77)$$

For component B,

$$\Delta G^B = \left(1 - \frac{T}{T_{mp}^B}\right)\Delta H_{fus}^B + \Delta C_{PB}\left[T - T_{mp}^B - T\,ln\frac{T}{T_{mp}^B}\right] + RT\left(ln\,x_B^l - ln\,x_B^s\right) + \left((1 - x_b)[a_1 x_a + b_1 x_a^2 + a_2 x_c + b_2 x_c^2 + 2c_2 x_b x_c^2] - b_1 x_a^2 x_b - b_2 x_b x_c^2 - c_2 x_b^2 x_c^2 - 2b_3 x_a x_c^2 - a_3 x_a x_c\right) - \left((1 - x_b)[a_1 x_a + a_2 x_c + b_2 x_c^2] - b_2 x_b x_c^2 - a_3 x_a x_c - 2b_3 x_a x_c^2\right) \quad (78)$$

And for component C,

$$\Delta G^C = \left(1 - \frac{T}{T_{mp}^C}\right)\Delta H_{fus}^C + \Delta C_{PC}\left[T - T_{mp}^C - T\,ln\frac{T}{T_{mp}^C}\right] + RT\left(ln\,x_C^l - ln\,x_C^s\right) + \left((1 - x_c)[a_2 x_b + 2b_2 x_b x_c + 2c_2 x_b^2 x_c + a_3 x_a + 2b_3 x_a x_c] - a_1 x_a x_b - 2b_1 x_a^2 x_b - c_2 x_b^2 x_c^2\right) - \left((1 - x_c)[a_2 x_b + 2b_2 x_b x_c + a_3 x_a + 2b_3 x_a x_c] - a_1 x_a x_b\right) \quad (79)$$

The *a*, *b*, and *c* coefficients within the first set of parentheses for each component are the liquid enthalpy of mixing empirical coefficients, while the coefficients within the last set of parentheses are the solid enthalpy of mixing empirical coefficients.

The final two equations which relate the concentrations of each component are

$$x_A^l + x_B^l + x_C^l = 1 \quad (80)$$

$$x_A^s + x_B^s + x_C^s = 1 \quad (81)$$

where the superscripts *l* and *s* stand for the liquid and solid phases, respectively. Solving these equations is discussed in the section below.

4.4 Numerical Method

A computer program was written in the numerical computing software MATLAB, to simultaneously solve the four binary simulation equations at various concentrations of each component. Due to the fact that there are five unknowns for the four equations, one of these unknowns must be inputted into the program. In order to solve these equations, certain properties of the pure salts must also be known. These include the molar mass, the melting temperature, the latent heat of fusion, and the specific heat in the liquid and solid phases. The values used are reproduced in table 1 below. These values were all assumed to be constant within the temperature range of the phase diagram. The inputted unknown is the liquid concentration of one of the components.

For instance, in the $NaNO_3$-KNO_3 system, the liquid concentration of KNO_3 is inputted into the program ranging from 1 to 99 percent mole KNO_3 (the percents 0 and 100 cannot explicitly be inputted, or the program will fail, but very small or very large mole percentages can be entered to estimate those values). The program will solve for the remaining four unknowns at each inputted composition, namely, the other liquidus concentration, the two solidus concentrations, and the temperature.

Solving these equations in MATLAB is accomplished using the built-in function solver called *fsolve*. It is used to solve systems of non-linear equations. The solver uses a trust-region dogleg algorithm to accomplish this. Information on this algorithm is provided by MATLAB. [19]. The equations are rewritten in the form

$$F(x) = 0 \tag{82}$$

and the solver will find the roots of the equations. Initial guesses need to be provided to the solver at each concentration, so the desired roots can be found more easily and accurately. The first guess is inputted manually because, for example, at 1 mole percentage KNO_3 in the $NaNO_3$-KNO_3 system, the solidification temperature and the relative amounts of the two solidus concentrations are all known (due to this concentration being so close to pure $NaNO_3$). After the solver outputs the roots to the equations at this concentration, it now uses these solutions as the initial guesses for the next concentration. And this is done throughout the whole range of inputted concentrations to ensure that the solver can find the roots quickly and efficiently.

To produce a full phase diagram the KNO_3 concentration is incremented by 1 mole percentage, starting from 1 and ending at 99 mole percent, with the calculations being performed at each increment. This data is then plotted to produce the simulated phase diagram.

As will be presented below, solutions to each of the three binary phase diagrams were not always continuous. Only in the $NaNO_3$-KNO_3 system were the solidus and liquidus lines continuous. For this system, the inputted concentration can be started at either end of the phase diagram and be continued all the way through to opposite side, and a solution will be found at each increment without the solver function failing to find a solution. Both the solidus and liquidus line both connect at the eutectic point, with a continuous slope on each side of the point.

This is not the case with either the $LiNO_3$-$NaNO_3$ or $LiNO_3$-KNO_3 systems. For these systems, each side of the phase diagram had to be solved separately. If the inputted concentration was ranged from 1 to 99 percent in a single run of the program, the solver would fail near concentrations past the eutectic point because it won't be able to find solution. If solutions were found, they would either include concentrations above unity or imaginary numbers, both of

which do not have any physical meaning. These roots were therefore discarded. So to solve for the phase diagrams of these system, each side of the diagram had to be solved independently. One script was written which inputted concentrations starting at the left side of the diagram, and another script starting at the right side of the diagram. The eutectic point of these two systems was determined to be the point of intersection between the two liquidus curves that were solved for separately. Also, the solidus curves in these systems showed a discontinuity in their slopes. They start out as curves but when they reach the eutectic temperature they become flat for a large range of compositions. But according to experimental data here and by others this is relatively common.

The salt property constants that were used for the modeling are shown in the table below.

Salt	Molar Mass (g/mol)	Melting Temperature (Kelvin)	Latent Heat (J/g)	$C_p(l) - C_p(s)$ (J/gK)
$NaNO_3$	84.9947	577.5	173	-0.11
KNO_3	101.103	607.4	96.6	-0.03
$LiNO_3$	68.946	525.9	363	0.25

Table 1. Salt property values

The molar mass values used are well documented. The melting temperatures as well as the latent heats (enthalpies of fusion) of the components were taken from a reference by Y. Takahashi et al. [17]. The specific heat differences between the liquid and solid states of the salts were those measured by M. J. Maeso and J. Largo [18].

Chapter 5. Results and Discussion

5.1 Binary System

The phase diagram predictions for all three binary systems were produced and compared against experimental data. The first comparisons are against the data collected at Dynalene Inc., by Kevin Coscia. The values of the empirical constants used for each system are shown in the table below.

Salt System	ΔH_{mix}, liquid			ΔH_{mix}, solid		
	a	b	c	a	b	c
$NaNO_3$:KNO_3	-1707	-284.5	0	6276	0	0
$LiNO_3$:$NaNO_3$	-1941.4	-2928.8	0	9204.8	3347.2	0
$LiNO_3$:KNO_3	-9183.9	-364	-1937.2	10460	4184	0

Table 2. Enthalpy of mixing empirical coefficient values

There is no *b* coefficient for the $NaNO_3$-KNO_3 solid enthalpy of mixing expression, due to the symmetry present in this system that is not seen in the other two mixtures. Additionally, the only binary system with a *c* coefficient is the $LiNO_3$-KNO_3 mixture, because it has the largest temperature difference between the eutectic temperature and pure component melting temperature. This extra coefficient enables a better fit between the predictions and experimental data shown here.

The sodium-potassium nitrate binary system is displayed in the figure below.

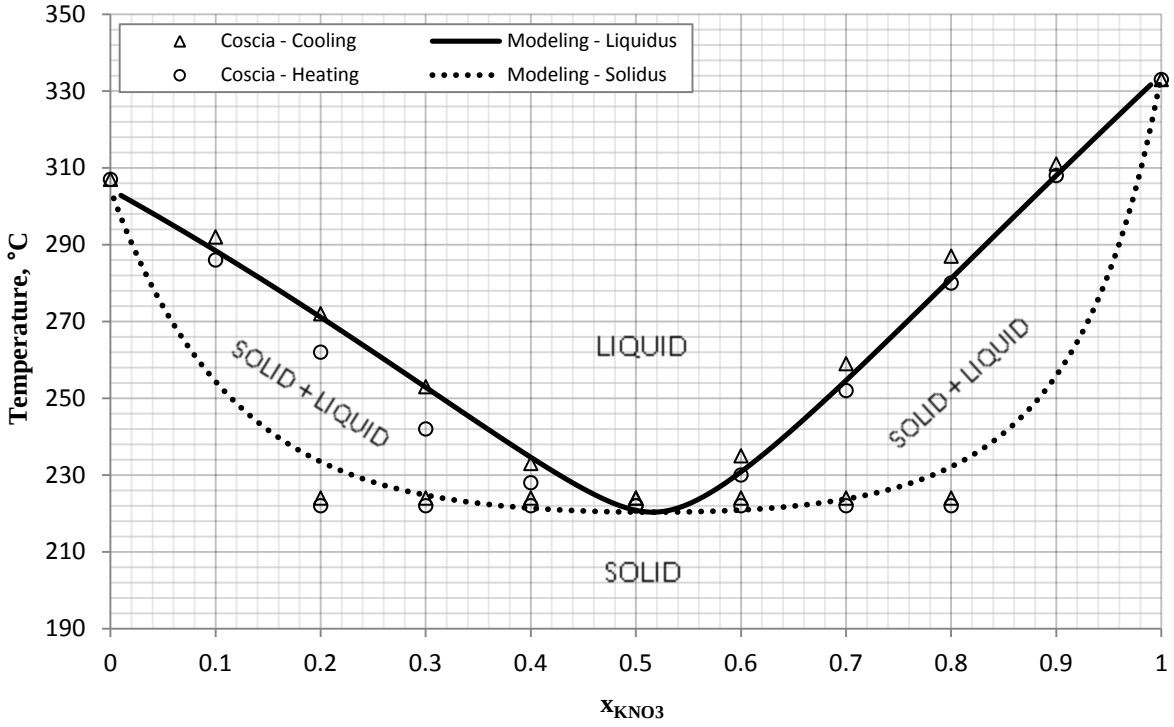

Figure 2. $NaNO_3$-KNO_3 simulated phase diagram compared against Coscia experimental data

Due to the continuous nature of this phase diagram, it displayed the closest fit to the experimental data. The data indicates a eutectic point is present at 50 mol% KNO_3 and 50 mol% $NaNO_3$ at a temperature of 222°C. The solid solubility of the system is also included; here it is seen as the group of data points at the eutectic temperature, ranging in composition from 20 mol% to 80 mol% KNO_3.

Using the thermodynamic model, the eutectic point was calculated to be at a temperature of 220.4°C with compositions of 52.1 mol% KNO_3 and 47.9 mol% $NaNO_3$. There is a minor discrepancy in the location of the eutectic point with the model predicting slightly more KNO_3 present and also at a faintly higher temperature. The predicted eutectic composition is within 5 percent error, while the predicted temperature is within 1 percent error.

The phase diagram for the $LiNO_3$–$NaNO_3$ binary system is displayed in the figure below. The eutectic temperature determined experimentally was 188°C at a composition of 44 mol%

$NaNO_3$ and 56 mol% $LiNO_3$. Again the solidus line is seen as the horizontal points ranging from 10 to 90 mol% $NaNO_3$, at the eutectic temperature.

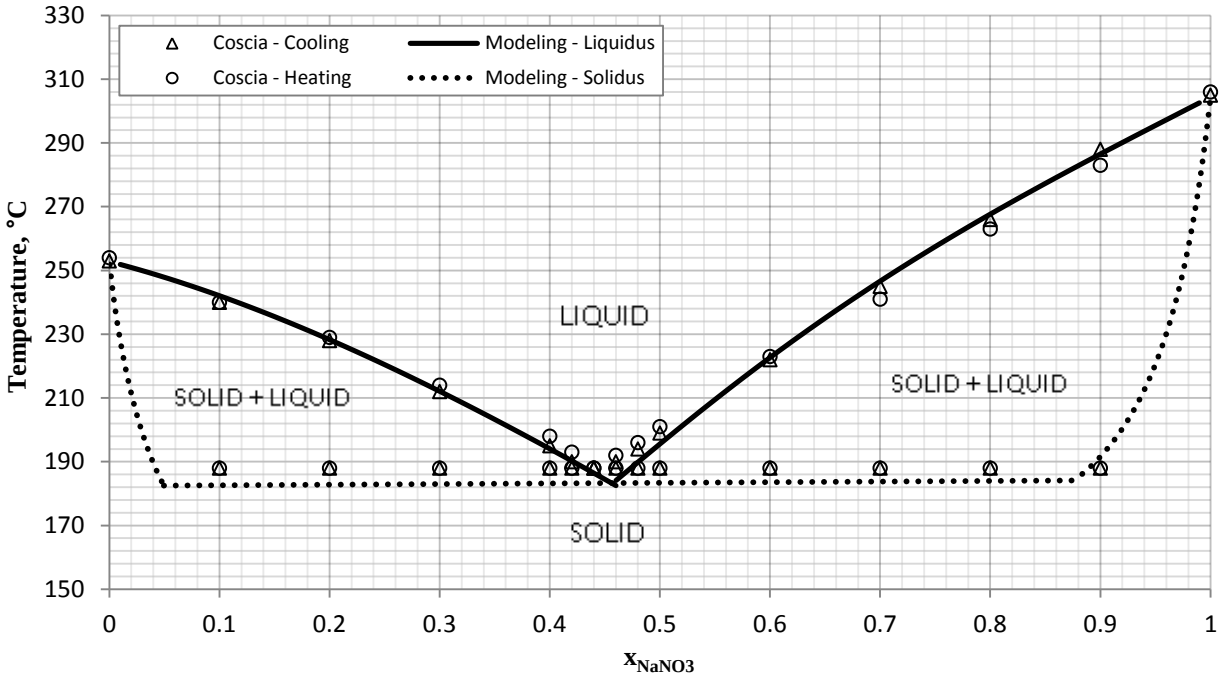

Figure 3. $LiNO_3$-$NaNO_3$ simulated phase diagram compared against Coscia experimental data

The simulated eutectic point was determined at a composition of 46 mol% $NaNO_3$ at 183°C. This eutectic composition had a larger value of $NaNO_3$ and the eutectic composition was at a lower temperature. The modeled eutectic composition was within 5 percent error of the experimental data and the modeled eutectic temperature are within 3 percent error of the experimental data.

The experimental data for the $LiNO_3$–KNO_3 binary system is displayed in the figure below. For this system the eutectic composition was experimentally determined to be 42.5 mol% $LiNO_3$ and 57.5 mol% KNO_3 at a temperature of 115°C. Again, the solidus line is constant at the eutectic temperature.

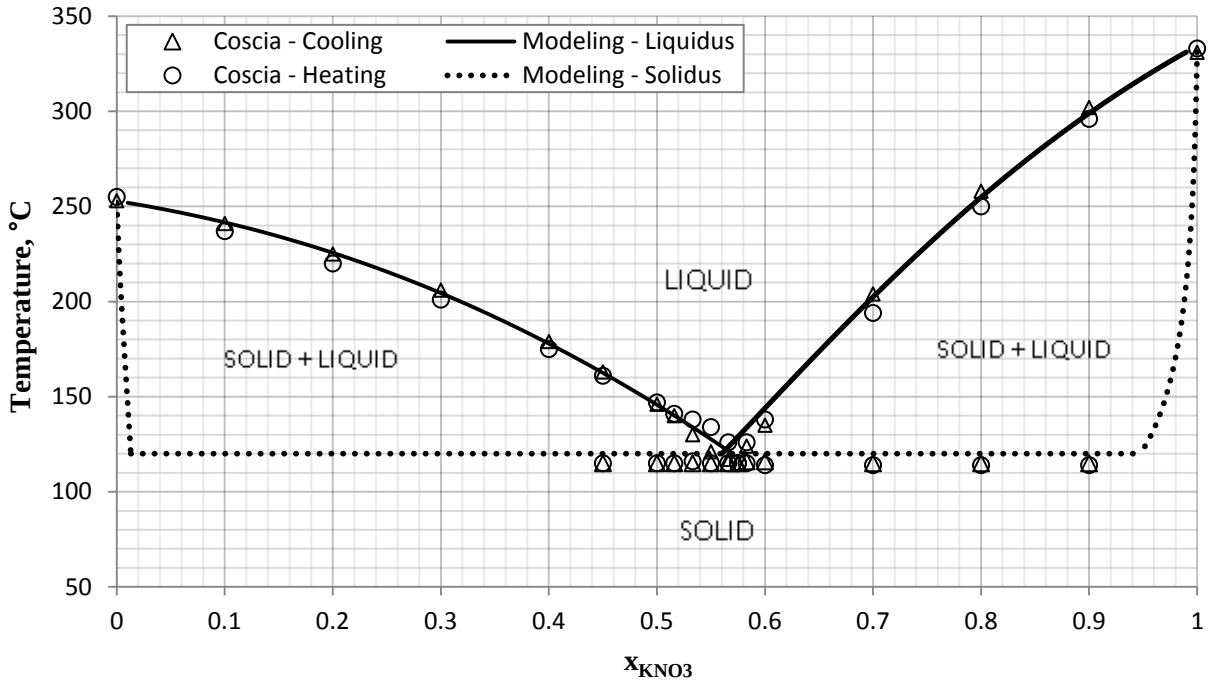

Figure 4. $LiNO_3$-KNO_3 simulated phase diagram compared against Coscia experimental data

The simulations produce a eutectic composition of 44 mol% $LiNO_3$ and 56 mol% KNO_3 at a temperature 122°C. Here, the predicted eutectic composition contains a lower amount of KNO_3, while the predicted eutectic temperature was greater. The calculated eutectic composition is within 3 percent error and the calculated temperature is within 5 percent error.

Each of these predicted phase diagrams showed great agreement with the experimental data that was collected. At compositions closer to the pure components, the agreement was excellent and a bit better than compared to compositions closer to the eutectic point, although the agreement near the eutectic point is still very good. The predicted phase diagrams will now be compared to experimental data recorded by others.

5.2 Binary Comparison with other Experimenters

The $NaNO_3$-KNO_3 system produced by Zhang et al. [11] is compared to our thermodynamic model's predictions. The results are shown below.

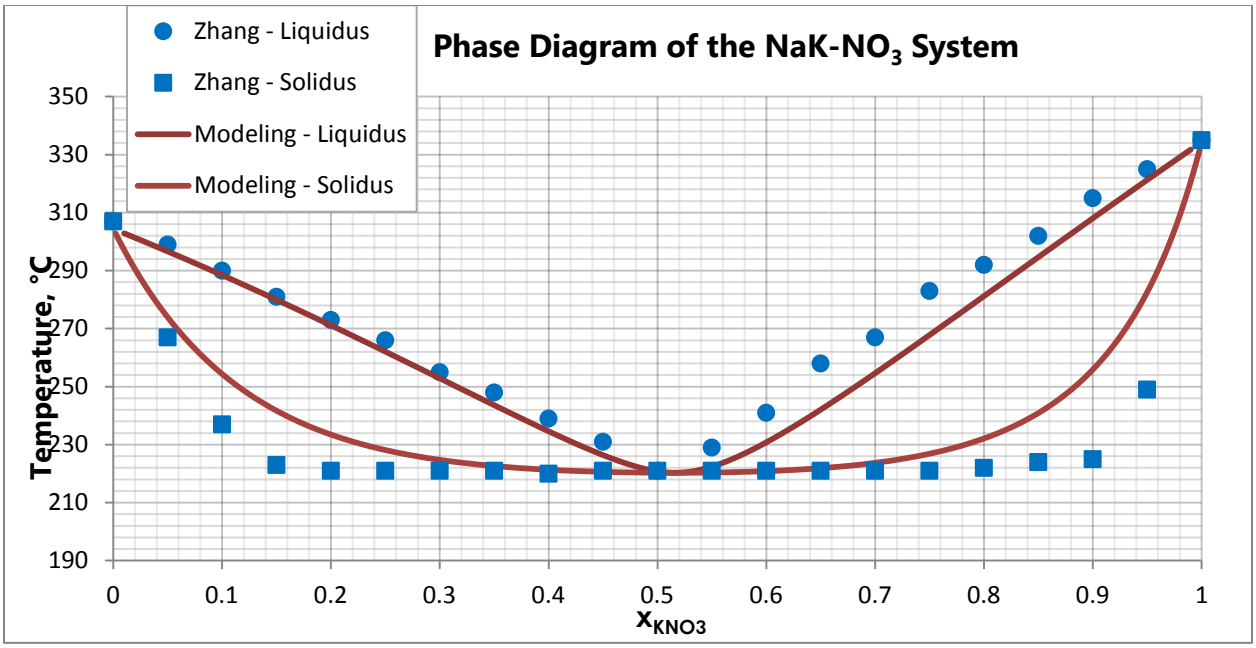

Figure 5. $NaNO_3$-KNO_3 simulated phase diagram compared against Zhang experimental data

The predicted eutectic composition and temperature are in very good agreement with Zhang. Some discrepancies do exist in both the liquidus and solidus curves. Zhang's data indicates that the liquidus values follows a near linear trend in contrast to the non-linear trend that our model produces. In addition he observed the solidus line as staying constant closer to each end of the phase diagram, whereas in our model the solidus follows a curved path.

Our predicted $LiNO_3$-$NaNO_3$ model is compared against the experimental data of both Campbell et al. [12] and Vallet [13].

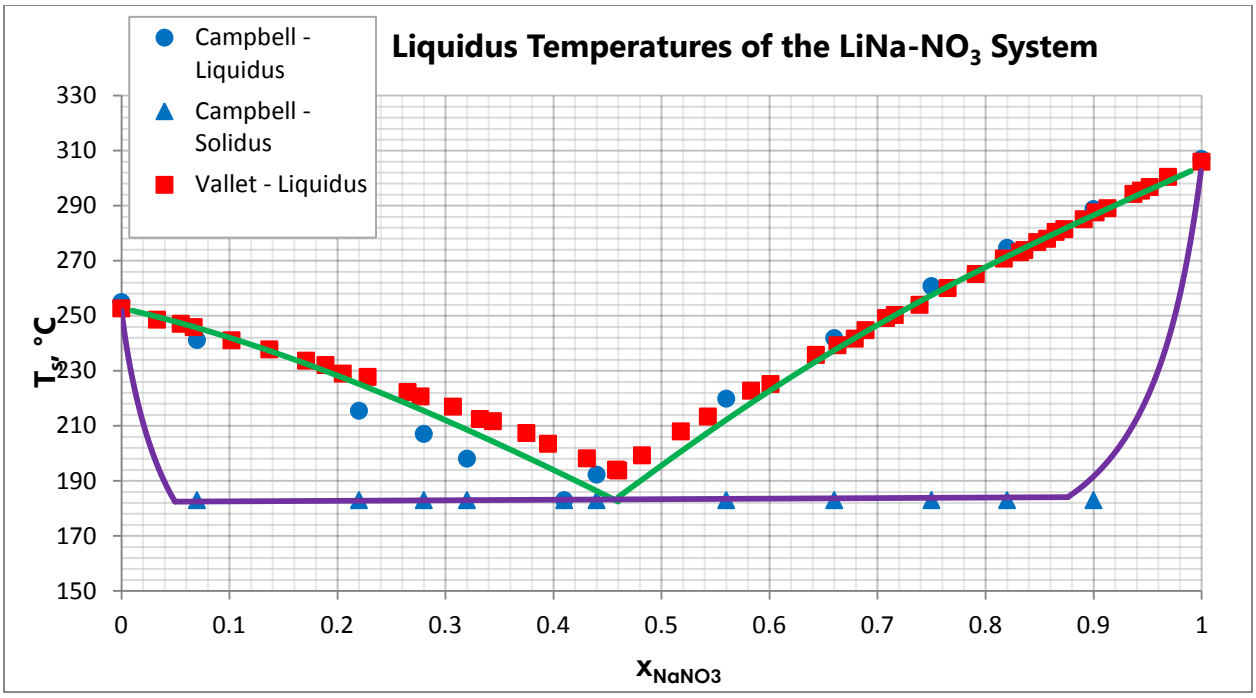

Figure 6. $LiNO_3$-$NaNO_3$ simulated phase diagram compared against Campbell and Vallet experimental data

Our predicted liquidus curve is in very good agreement with both Vallet's and Campbell's experimental data. There are some minor disagreements with the coordinates of the eutectic point, however. Vallet's reported the eutectic at 46 mol% $NaNO_3$ agrees with the predictions here but the temperature is higher than ours. Campbell reported his eutectic at a temperature similar to ours but at a composition of 41 mol% $NaNO_3$. Vallet did not report solidus data but Campbell's solidus data matches up very well with our predicted solidus curve. It should be noted that Vallet and Campbell used constantly mixed systems and observational techniques rather than differential scanning calorimetry, which may be the reason for the discrepancy in eutectic data.

And finally our simulated $LiNO_3$-KNO_3 phase diagram is compared against experimental data from Vallet [12] and Zhang et al. [10].

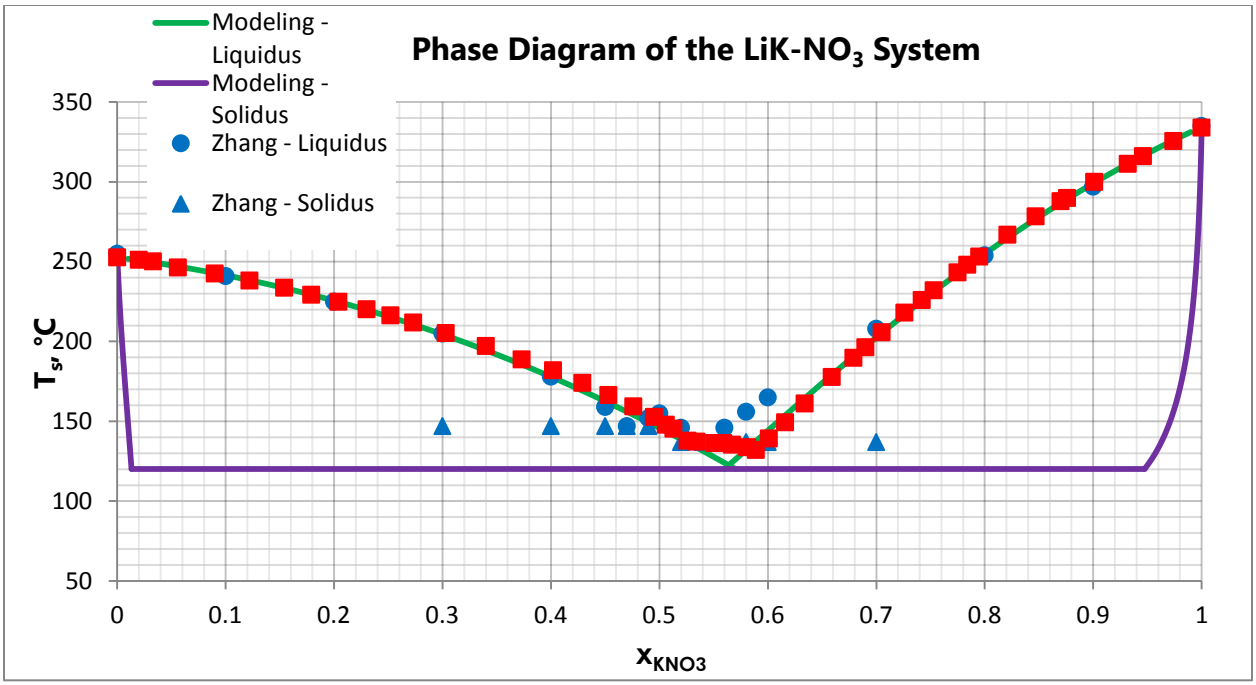

Figure 7. $LiNO_3$-KNO_3 simulated phase diagram compared against Zhang and Vallet experimental data

Similarly, our model is in good agreement with the data of both Vallet and Zhang, but some discrepancies near the eutectic are present. Vallet reported a eutectic temperature of 132.1°C at 58.1 mol% KNO_3 and Zhang reported a eutectic temperature of 137°C at 54 mol% KNO_3. Our predicted eutectic composition lies between Vallet's and Zhang's at 56 mol% KNO_3 but at a lower temperature of 122°C. Additionally, Zhang reported a discontinuity in the solidus line around 52 mol% KNO_3, but neither our simulation nor data collection observed any discontinuities in this system.

5.3 Ternary System Simulation Results

The ternary prediction results are as follows. The graph below shows modeling for mole percent values of $LiNO_3$ of 0%, 10%, 20%, 30%, 35%, 38%, 40%, and 43%.

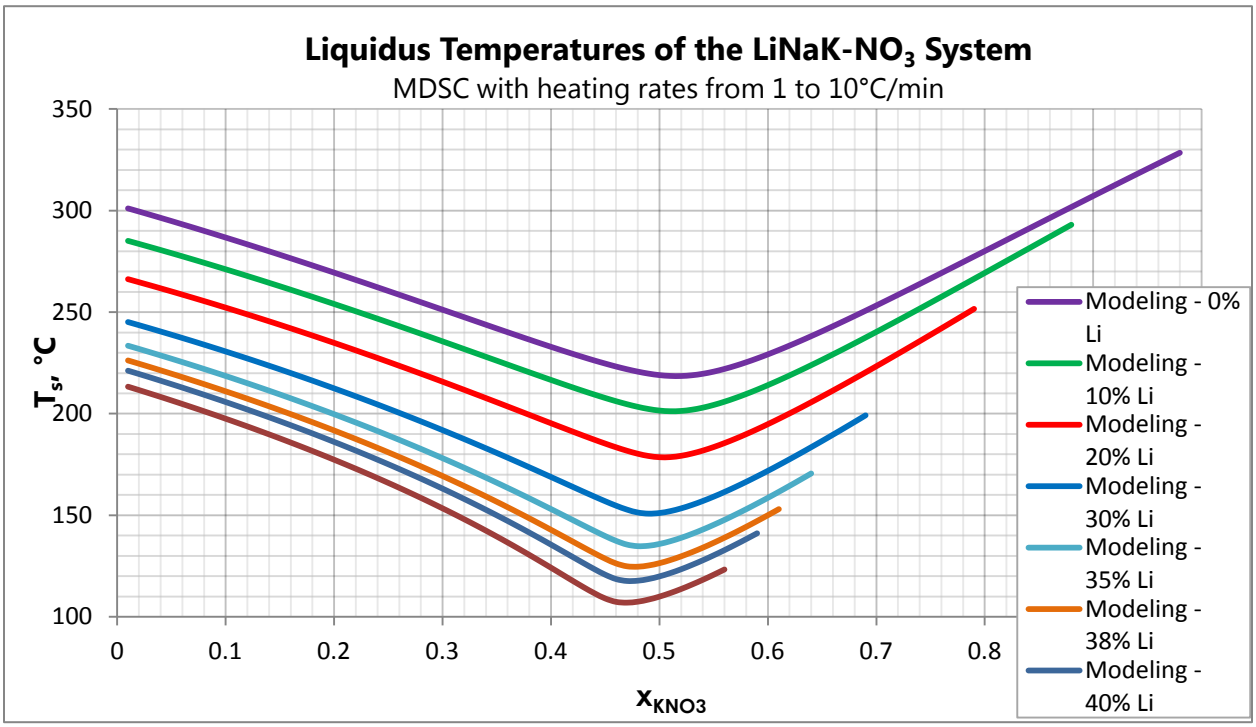

Figure 8. $LiNO_3$-$NaNO_3$-KNO_3 System Predicted Phase Diagram - Lower Values

When viewing this figure, it should be noted that as the quantity of $LiNO_3$ in the system increases, the resulting liquidus curve is shorter than the previous one. So naturally, at 40 mol% $LiNO_3$ for example, the value of KNO_3 (or $NaNO_3$) can only range from 0-60 mol%. Here, as the value of $LiNO_3$ increases, the liquidus curves shift down in temperature and also the corresponding eutectic point on each curve shifts to the left. This is the case for values of $LiNO_3$ up to 43 mol%. The curves are smooth and continuous. The eutectic composition and temperature turn out to be at a concentration of 43-47-10 mole percents of $LiNO_3$-KNO_3-$NaNO_3$ respectively at a temperature of 107° Celsius.

The below figure shows the predictions for $LiNO_3$ mole percentage values of 45%, 50%, 54%, 60%, 70%, 80%, and 90%.

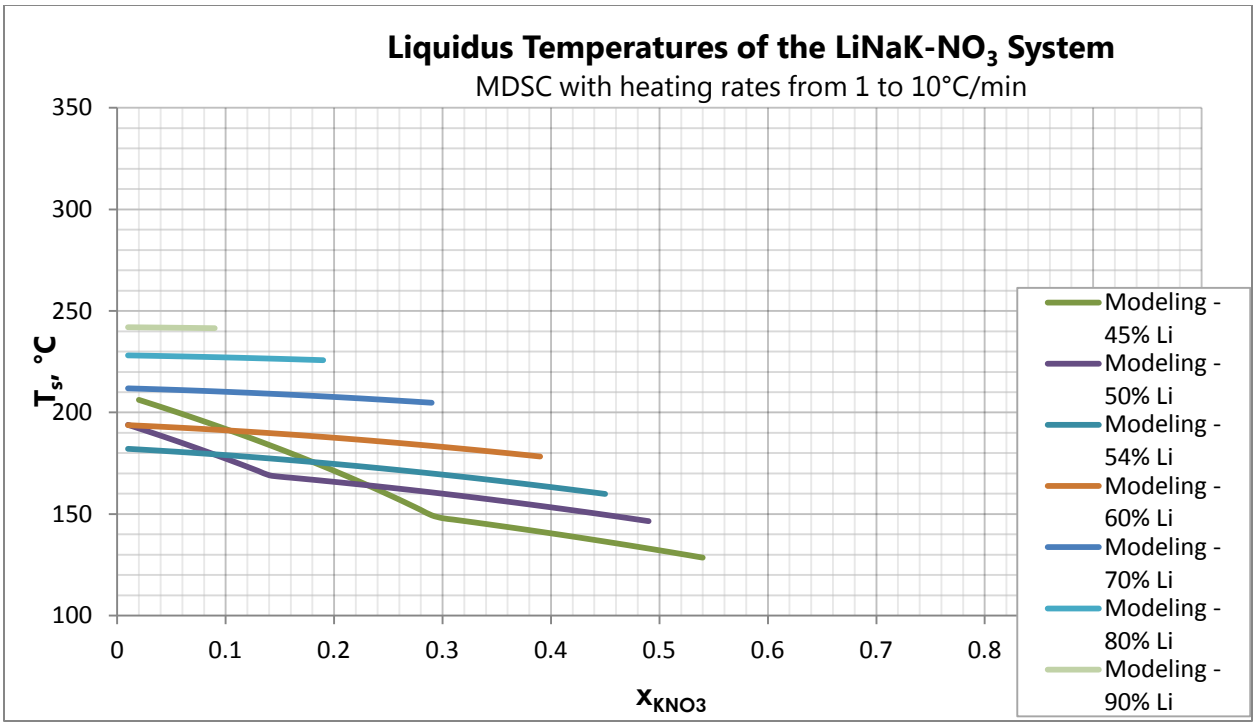

Figure 9. $LiNO_3$-$NaNO_3$-KNO_3 System Predicted Phase Diagram - Higher Values

Modeling past 43 mol% $LiNO_3$ and the liquidus curves follow a new trend. At 43 mol% $LiNO_3$ the liquidus curve is continuous and is a smooth concave curve. But at 45 mol% $LiNO_3$ as seen above, this is not the case; there is a discontinuity in the slope of these curves. The liquidus curve is convex, and two sides of the curve meet together with separate slopes. This convex nature is also seen in the 50 mol% $LiNO_3$ curve. The phenomenon is identified at concentrations of $LiNO_3$ from 44-53 mol%. The likely cause of this is the increased addition of $LiNO_3$. In the $NaNO_3$-KNO_3 binary system, the liquidus curve is concave, while in both of the binary systems with $LiNO_3$, the liquidus is convex. The reason for this has to do with the chemistry of each system. Additionally, these liquidus curves are at higher temperatures compared to the 43 mol% $LiNO_3$ curve, and they shift up as the $LiNO_3$ is increased.

At concentrations above 53 mol% $LiNO_3$, the liquidus curve slopes become continuous again and begin to flatten out, especially at much higher concentrations. These curves are neither

concave nor complex, but rather they range from the binary temperature at one side of the phase diagram, to the binary temperature at the other side of the phase diagram. This is more apparent at higher $LiNO_3$ concentrations namely, the modeling from 60 mol% $LiNO_3$ to 90 mol% $LiNO_3$. The suspected reason for this is that at these high concentrations, the liquidus curve is equivalent to one side of the liquidus curve in the corresponding binary system. In the binary systems with $LiNO_3$, the liquidus curves had to be solved from both sides separately, and the curves here are simply one of these sides. To ensure the accuracy of these curves the temperature at the end of each liqudus line was checked against the temperature of the corresponding binary system, which validated the curves.

In addition to the liquidus curves that are presented above, the solidus lines are also solved for in the ternary system. The solidus lines of the ternary mixture are shown at the following concentrations of $LiNO_3$: 0 mole percent, 30 mole percent, and 43 mole percent.

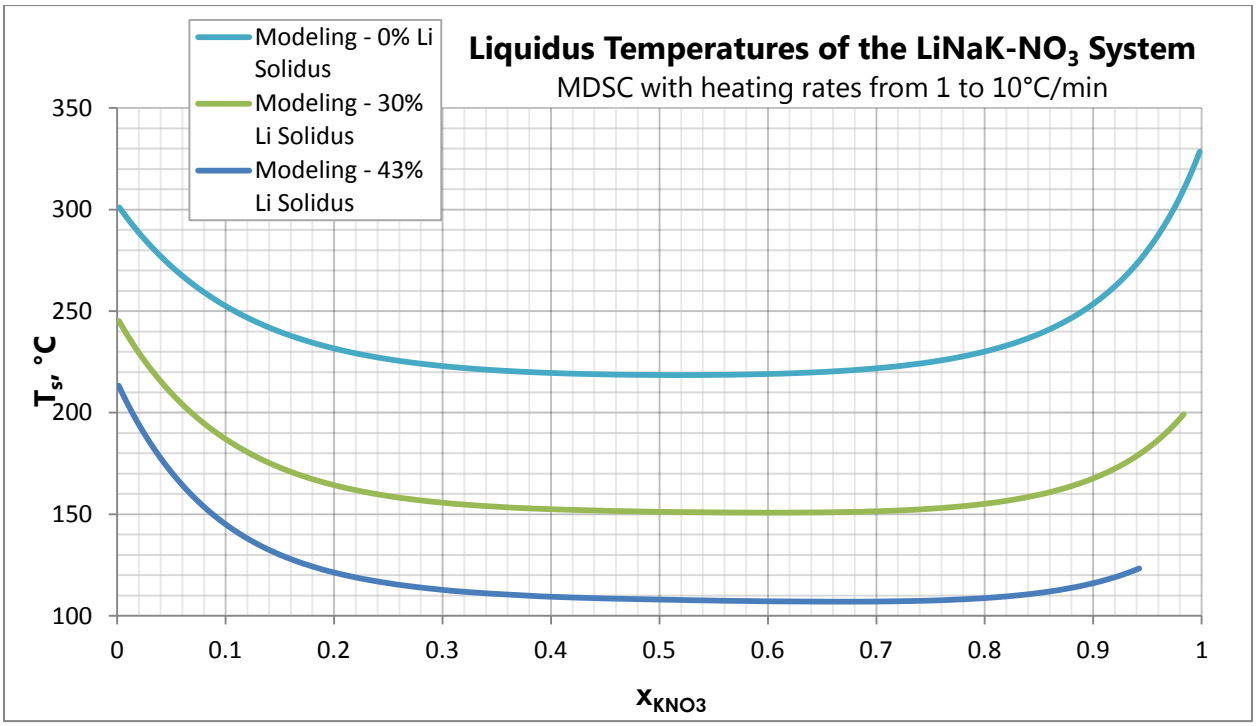

Figure 10. $LiNO_3$-$NaNO_3$-KNO_3 System Predicted Liquidus and Solidus Curves

The figure above represent slices of the full ternary system's phase diagram and does not show the full picture. Because the $NaNO_3$- KNO_3- $LiNO_3$ consists of three components, the complete phase diagram is depicted as a surface plot, and is shown at different views in the figures below.

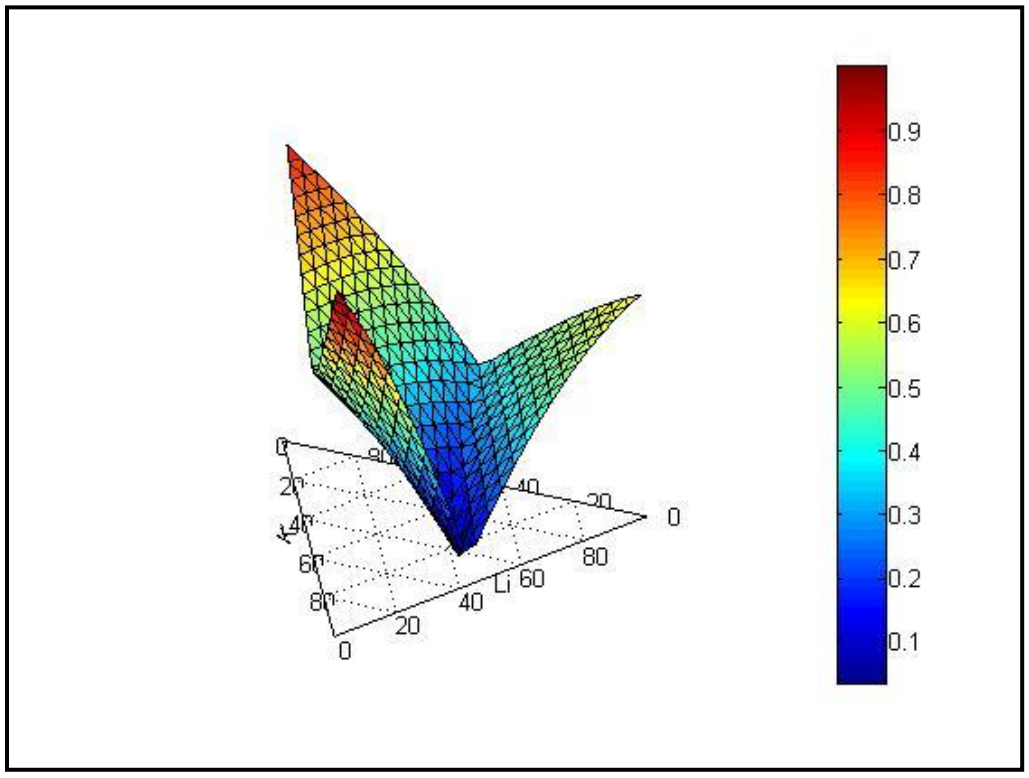

Figure 11a. Ternary phase diagram surface plot

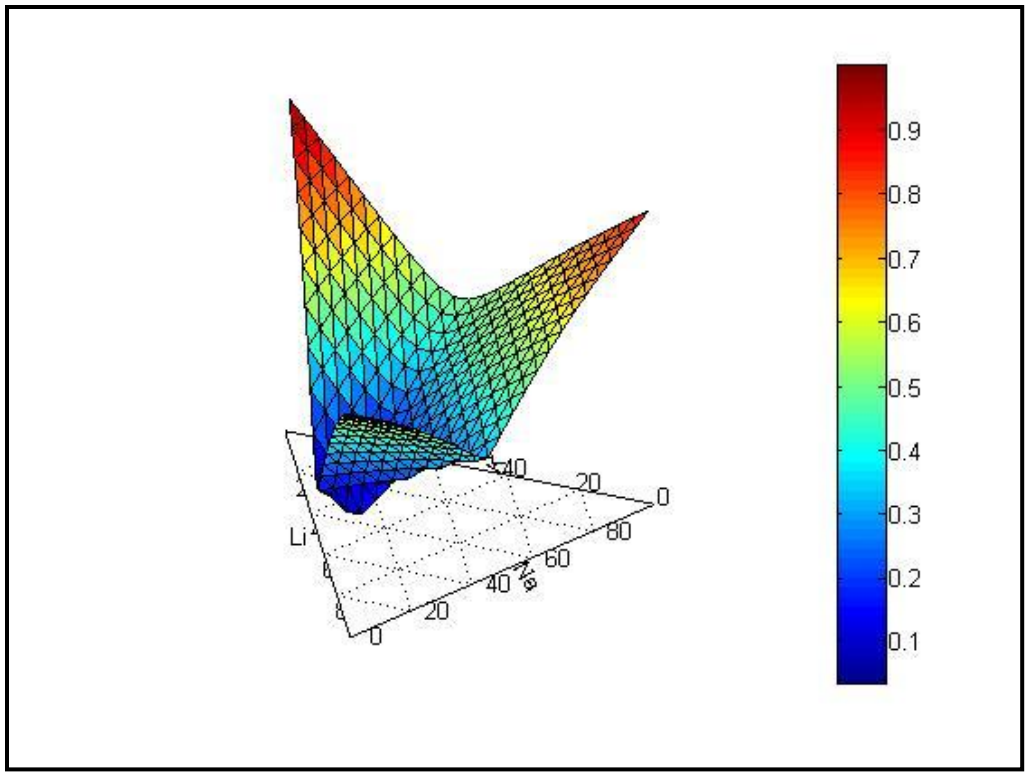

Figure 11b. Ternary phase diagram surface plot

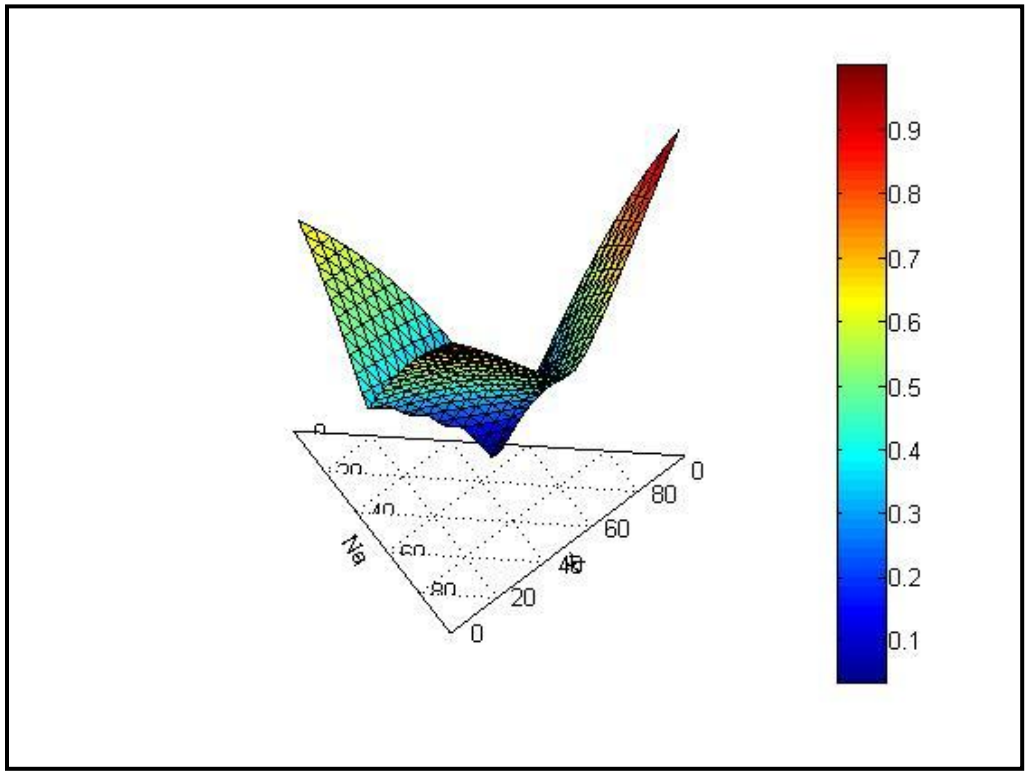

Figure 11c. Ternary phase diagram surface plot

The temperature bar on the right of the figures represents the normalized temperature ranging from zero to one, where the highest temperature is 328.5°C and the lowest temperature is 107°C. The three eutectic points of the binary systems are observed as the valleys at each of the three edges of the ternary triangle. The top view of this surface shows the variation of temperature as the concentration changes.

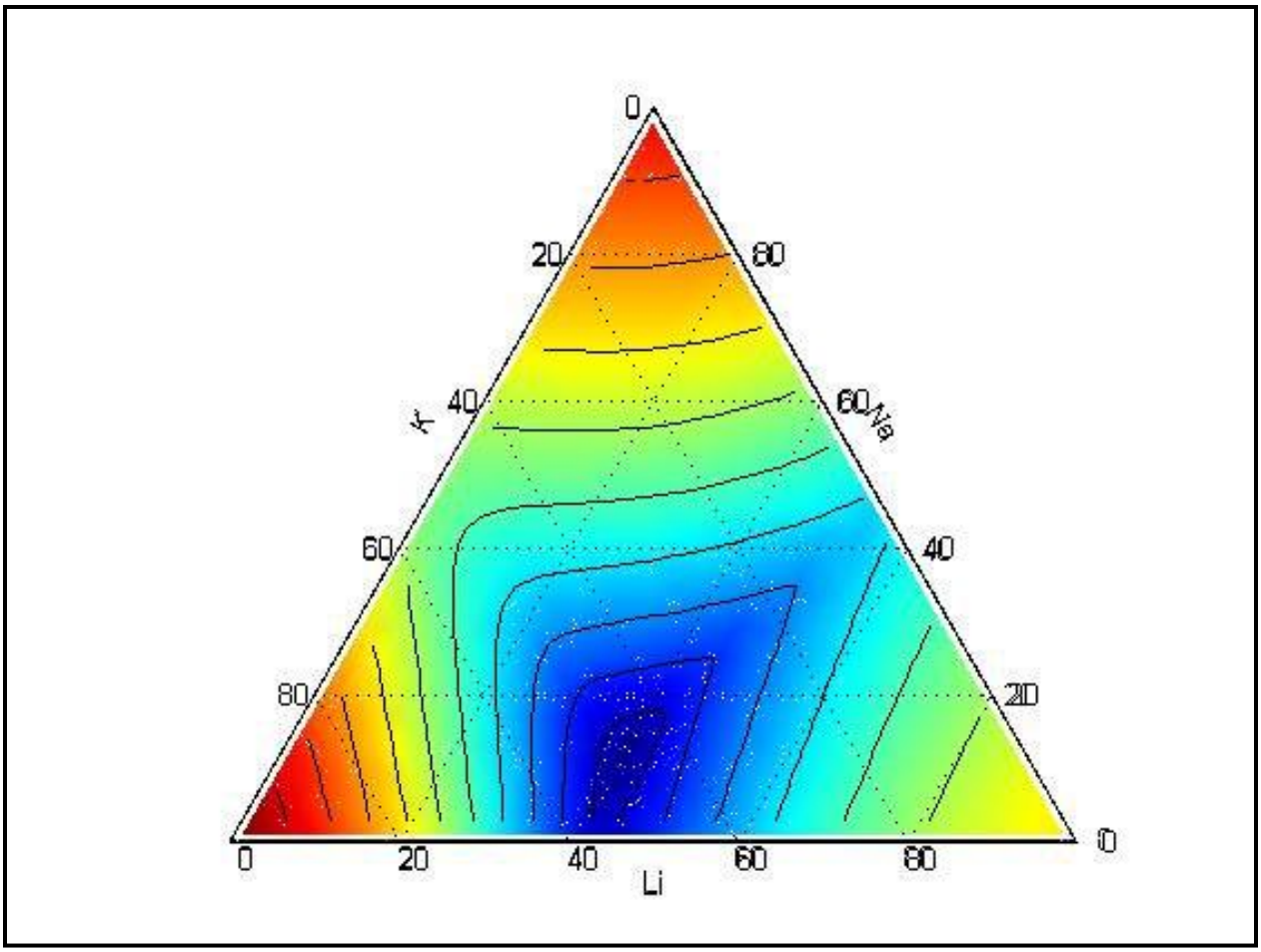

Figure 12. Top view of ternary phase diagram

The ternary system eutectic point and the surrounding compositions can be seen at as the darkest blue portion of this figure. The highest temperatures occur at compositions near pure KNO_3 and pure $NaNO_3$. Contour lines are also added to show where the variations in the temperatures are present.

5.4 Ternary System Comparison Results

The ternary prediction results are now compared to experimental data that was collected. The modeling will be split into separate graphs so the comparison with experimental data will be easier to observe. First, comparisons at low concentrations of $LiNO_3$, can be seen in the figure below.

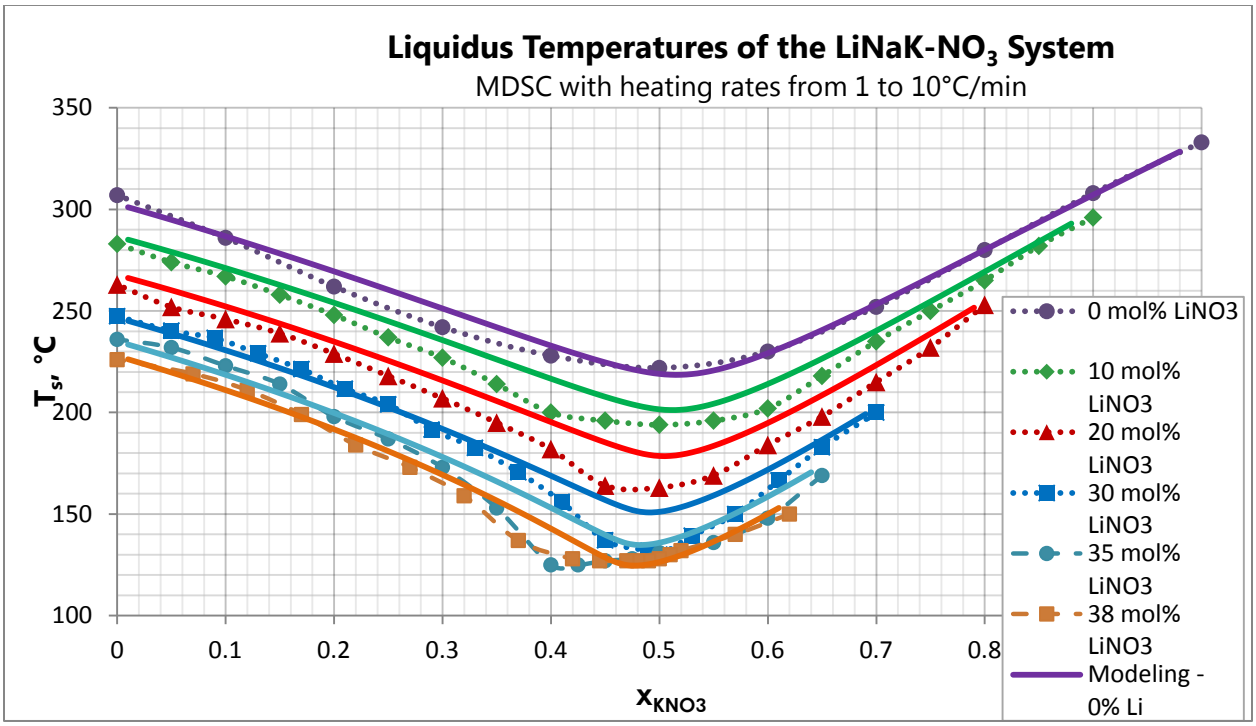

Figure 13. $LiNO_3$-$NaNO_3$-KNO_3 simulated phase diagram compared against experimental data, low $LiNO_3$ values

The predicted values match up well with the experimental data at low concentrations but at concentrations of 20 and 30 mol% KNO_3, a discrepancy is observed near the eutectic points of the curves. This difference decreases at 35 mol% $LiNO_3$, and at 38 mol% $LiNO_3$ the model and experimental data match very well, except for a minor disagreement around 40 mol% KNO_3.

The next graph shows the model at higher concentrations of $LiNO_3$.

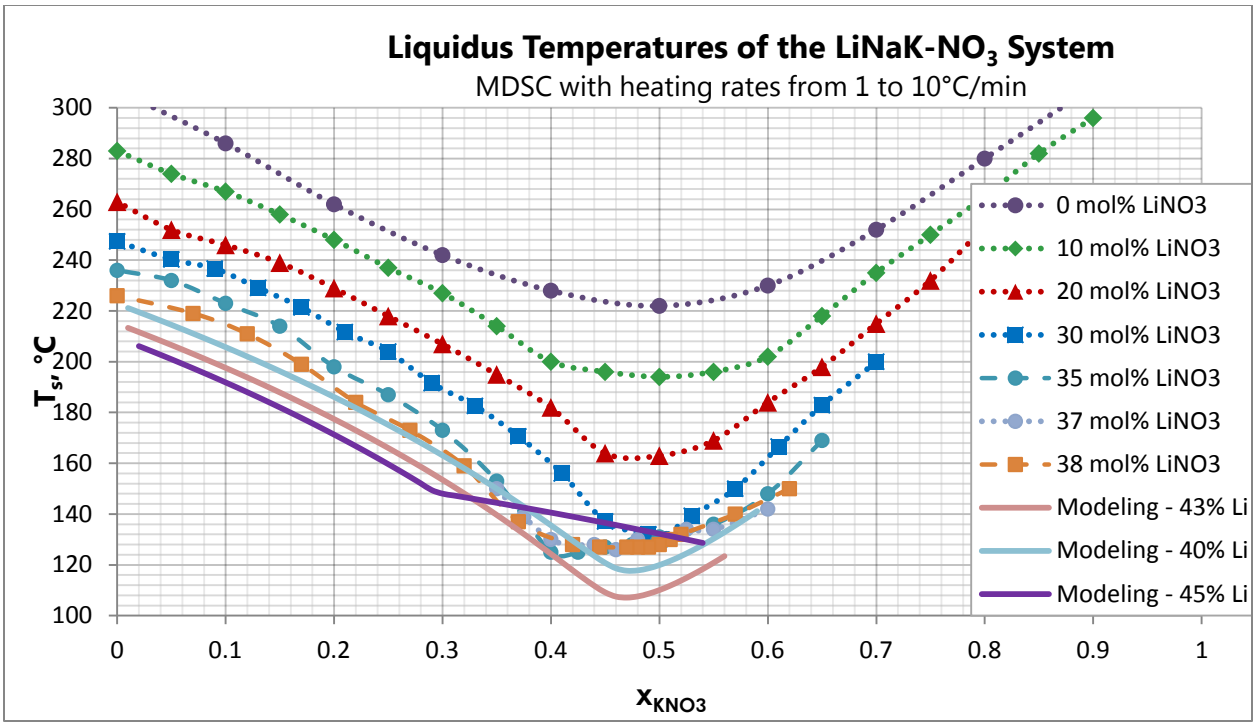

Figure 14. $LiNO_3$-$NaNO_3$-KNO_3 simulated phase diagram compared against experimental data, eutectic $LiNO_3$ values

The simulations are produced at 40, 43, and 45 mol% $LiNO_3$. First, the modeling at 40 mol% $LiNO_3$ is at temperatures below the experimental data at 38 mol% $LiNO_3$ which is expected. Modeling the increase in $LiNO_3$ up to 43 mol% follows the same manner, reaching the eutectic point as described above. And at 45 mol% $LiNO_3$, the discontinuous nature in the slope of the liquidus curve is observed, which was explained earlier.

The results above give an informative idea to the behavior of these salt mixtures. The next step would be to use these results and apply them to real-world applications. For instance, companies who would make use of these molten nitrate salts as heat transfer fluids, this information can be used to make cost-effective decisions.

Lower melting points, as discussed above, is an important characteristic in heat transfer fluids for concentrated solar power plants. Using a composition that is not near the eutectic point

of a certain system would be a waste of resources for that company. In addition, the cost of each of these salts are of interest for companies. If the cost of each of these three salts were identical, obviously choosing the system with the lowest eutectic temperature (the ternary system in this case), would be the logical choice. But, if one component is more expensive than the others, one might not just choose the eutectic composition blindly, but might choose a composition that has a higher melting temperature but less of the more expensive component if this will reduce the cost for a company in the long run.

Chapter 6. Conclusions

The present work illustrates the modeling of phase diagrams of selected binary and ternary nitrate salts. The results presented validate the use of the Gibbs energy minimization model used. The phase diagram simulations matched well with the experimental data collected here and with data gathered by other researchers. For the binary systems, the thermodynamic model that was used involved setting the liquid and solid phases equal to each other. Because of this, when solving the resulting equations, both the liquidus and solidus curves were produced. The same model was used for the ternary system. Here though, only those empirical coefficients used for each binary mixture were needed to accurately model the ternary phase diagram. This demonstrates that the binary interactions between the salts have a much larger influence than the ternary interaction. The equations were solved using a built-in MATLAB solver function, which simultaneously solves the resulting coupled non-linear set of equations at each inputted concentration. The eutectic points of each system was determined, with the $LiNO_3$-KNO_3 binary system having the lowest predicted binary temperature of 122° Celsius. The binary simulations agree very well with the experimental data collected by our group using differential scanning calorimetry. The predicted ternary eutectic point was determined to be at a composition of 43 mol% $LiNO_3$, 47 mol% KNO_3, and 10 mol% $NaNO_3$ with the temperature bring 107° Celsius. The ternary phase diagram also is in reasonable agreement with the data collected by our group.

It should be noted that the strategy used to model these phase diagrams is not trivial. Many different methods and procedures exist, some of which were attempted, with less than satisfactory findings. Using the Gibbs function is a common theme, but in representing the interactions between the components, numerous approaches exist. Possessing a thermodynamic

model which can accurately predict the phase diagrams of binary and ternary mixtures is a valuable asset to researchers as well as concentrated solar power companies.

Chapter 7. Further Research

Further research into the thermodynamic models presented should include treating the salt's properties such as specific heat and latent heats, not as constants, but as functions of temperature. This may have the effect of improving the simulations. Another interesting analysis that could be conducted would be to investigate how changes in the binary coefficients would affect the ternary phase diagram simulations. For example, choosing coefficients which may not produce an accurate binary simulation but will better match the ternary experimental data may be found. Conducting research into the possible effect of the addition of the ternary interaction between the three components, when modeling the ternary mixture should be done. This was assumed to be negligible in our models. The addition of other alkali metals should also be studied, such as rubidium or cesium. Alkaline nitrates could also be included in this research. Additionally, this thermodynamic model is not unique to nitrate systems, but could also be applied to other anion systems, for example halides. Use of these different compounds can provide further verification of the model. Lastly, using this formulation for higher-order systems, four or five components systems for instance, should be investigated.

List of References

1. B. K. Hodge. *Alternative Energy Systems and Applications.* 2010. John Wiley and Sons Inc., Print.

2. Robert W. Bradshaw. *Viscosity of Multi-component Molten Nitrate Salts - Liquidus to 200°C.* 2010. Sandia National Laboratories, pp. 1-21.

3. M. L. McGlashan. *Chemical Thermodynamics.* 1979. Academic Press Inc, pp. 268. Print.

4. I. Prigogine, R. Defay. *Chemical Thermodynamics.* 1973. Longman Group Limited, London, pp.177-178. Print.

5. C. M. Kramer, C. J. Wilson. *The Phase Diagram of $NaNO_3$-KNO_3.* 1980. Thermochimica Acta, 42, pp. 253-264.

6. O. J. Kleppa, L.S. Hersh. *Heats of Mixing in Liquid Alkali Nitrate Salt Systems.* 1961. The Journal of Chemical Physics, Vol. 34, No. 2, pp. 351-358.

7. P. Jablonski, A. Muller-Blecking, W. Borchard. *A Method to Determine Mixing Enthalpies By DSC.* 2003. Journal of Thermal Analysis and Calorimetry, Vol. 74, pp. 779-787.

8. P. J. Spencer. *A Brief History of CALPHAD.* 2008. Computer Coupling of Phase Diagrams and Thermochemistry 32, pp. 1-8.

9. O. J. Kleppa, L.S. Hersh. *Calorimetry in Liquid Thallium Nitrate-Alkali Nitrate Mixtures.* 1962. The Journal of Chemical Physics, Vol. 36, No. 2, pp. 544-547.

10. Xuejun Zhang, Kangcheng Xu, Yici Gao. *The Phase Diagram of $LiNO_3$-KNO_3.* 2002. Thermochimica Acta, 385, pp. 81-84.

11. Xuejun Zhang, Jun Tian, Kangcheng Xu, Yici Gao. *Thermodynamic Evaluation of Phase Equilibria in $NaNO_3$-KNO_3 System.* 2003. Journal of Phase Equilibria, Vol. 24, No. 5, 441-446.

12. A. N. Campbell, E. M. Kartzmark, M. K. Nagarajan. *The Binary (Anhydrous) Systems of $NaNO_3$-$LiNO_3$, $LiClO_3$-$NaClO_3$, $LiClO_3$-$LiNO_3$, $NaNO_3$-$NaClO_3$ and the Quaternary System of $NaNO_3$- $LiNO_3$-$LiClO_3$-$NaClO_3$.* 1962. Canadian Journal of Chemistry, 40, pp. 1258-1265.

13. C. Vallet. *Phase Diagrams and Thermodynamic Properties of some Molten Nitrate Mixtures.* 1972. Journal of Chemical Thermodynamics, 4, pp. 105-114.

14. A. G. Bergman, K. Nogoev. *The $CO(NH_2)_2$-$LiNO_3$; K, Li, Na || NO_3; and K, NH_4, Na || NO_3 Systems.* 1964. Russian Journal of Inorganic Chemistry, Vol. 9, No. 6, 771-773.

15. K. Coscia, S. Nelle, T. Elliott, S. Mohapatra, A. Oztekin, S. Neti. *The Thermophysical Properties of the Na-K, Li-Na, and Li-K Nitrate Salt Systems.* 2011. ASME Conference IMECE

16. K. Coscia, S. Nelle, T. Elliott, S. Mohapatra, A. Oztekin, S. Neti. *The Heat Transfer Characteristics and Phase Diagram Modeling of Molten Binary Nitrate Salt System.* 2011. SolarPACES Conference.

17. Y. Takahashi, R. Sakamoto, M. Kamimoto. *Heat Capacities and Latent Heats of $LiNO_3$, $NaNO_3$, KNO_3.* 1988. International Journal of Thermophysics, Vol. 9, No. 6, 1081-1090.

18. M. J. Maeso and J. Largo. *Phase Diagrams of $LiNO_3$-KNO3 and $LiNO_3$-KNO_3: the Behaviour of Liquid Mixtures.* 1993. Thermochimica Acta, 223, pp. 145-156.

19. The Mathworks, Inc. *Equation Solving Algorithms.* http://www.mathworks.com/help/toolbox/optim/ug/brnoyhf.html

Vita

Tucker is the son of Walter T. and PattiAnn Elliott and was born on March 18, 1988. He grew up in Huntington, New York. He received his Bachelor of Science in mechanical engineering with high honors from Lehigh University in May of 2010. As a presidential scholar, he continued his education at Lehigh, and will receive his Master of Science in mechanical engineering in January of 2012.